UHMK1 is a novel splicing regulatory kinase

Received for publication, June 1, 2022, and in revised form, January 18, 2023 Published, Papers in Press, February 18, 2023,
https://doi.org/10.1016/j.jbc.2023.103041

Vanessa C. Arfelli[1], Yun-Chien Chang[2], Johannes W. Bagnoli[3], Paul Kerbs[4,5,6], Felipe E. Ciamponi[7], Laissa M. da S. Paz[1], Serhii Pankivskyi[8], Jean de Matha Salone[8], Alexandre Maucuer[8], Katlin B. Massirer[7], Wolfgang Enard[3], Bernhard Kuster[2], Philipp A. Greif[4,5,6], and Leticia Fröhlich Archangelo[1,*]

From the [1]Department of Cellular and Molecular Biology and Pathogenic Bioagents, Ribeirão Preto Medical School, University of São Paulo (FMRP-USP), Ribeirão Preto, São Paulo, Brazil; [2]Proteomics and Bioanalytics, School of Life Sciences Weihenstephan, Technical University of Munich (TUM), Freising, Germany; [3]Anthropology & Human Genomics, Department of Biology II, Ludwig-Maximilians-University (LMU), Martinsried, Germany; [4]Laboratory for Experimental Leukemia and Lymphoma Research, Munich University Hospital, Ludwig-Maximilians University (LMU), Munich, Germany; [5]German Cancer Consortium (DKTK), partner site Munich, Munich, Germany; [6]German Cancer Research Center (DKFZ), Heidelberg, Germany; [7]Center for Medicinal Chemistry (CQMED), Center for Molecular Biology and Genetic Engineering (CBMEG), University of Campinas (UNICAMP), Campinas, São Paulo, Brazil; [8]SABNP, Univ Evry, INSERM U1204, Université Paris-Saclay, Evry, France

Reviewed by members of the JBC Editorial Board. Edited by Ronald Wek

The U2AF Homology Motif Kinase 1 (UHMK1) is the only kinase that contains the U2AF homology motif, a common protein interaction domain among splicing factors. Through this motif, UHMK1 interacts with the splicing factors SF1 and SF3B1, known to participate in the 3′ splice site recognition during the early steps of spliceosome assembly. Although UHMK1 phosphorylates these splicing factors *in vitro*, the involvement of UHMK1 in RNA processing has not previously been demonstrated. Here, we identify novel putative substrates of this kinase and evaluate UHMK1 contribution to overall gene expression and splicing, by integrating global phosphoproteomics, RNA-seq, and bioinformatics approaches. Upon UHMK1 modulation, 163 unique phosphosites were differentially phosphorylated in 117 proteins, of which 106 are novel potential substrates of this kinase. Gene Ontology analysis showed enrichment of terms previously associated with UHMK1 function, such as mRNA splicing, cell cycle, cell division, and microtubule organization. The majority of the annotated RNA-related proteins are components of the spliceosome but are also involved in several steps of gene expression. Comprehensive analysis of splicing showed that UHMK1 affected over 270 alternative splicing events. Moreover, splicing reporter assay further supported UHMK1 function on splicing. Overall, RNA-seq data demonstrated that UHMK1 knockdown had a minor impact on transcript expression and pointed to UHMK1 function in epithelial-mesenchymal transition. Functional assays demonstrated that UHMK1 modulation affects proliferation, colony formation, and migration. Taken together, our data implicate UHMK1 as a splicing regulatory kinase, connecting protein regulation through phosphorylation and gene expression in key cellular processes.

Phosphorylation is a reversible and dynamic post-translational modification mediated by kinases and counteracted by phosphatases. It is essential for the regulation of signaling networks that govern most of the cellular and physiologic processes, such as protein synthesis, cell growth and division, metabolism, inflammation, development, and aging (1).

The U2AF Homology Motif Kinase 1 (UHMK1) is the only kinase known to contain the U2AF homology motif (UHM) (2). UHM motifs share a high level of sequence identity with the canonical RNA recognition motif, which mediates protein–RNA interactions and is often found in RNA-binding proteins. However, specific sequences within the UHM motif enable protein–protein instead of protein–RNA interactions. It has been proposed that UHMs evolved from RRMs and connect mRNA processing to other nuclear events (3).

UHMK1 is a serine/threonine kinase that preferentially phosphorylates proline-directed serine residues (4). UHMK1 phosphorylates the splicing factors SF1 and SF3B1 *in vitro* (4, 5) and interacts with UHM ligand motifs (ULMs) found in both factors (5). SF1 is responsible for recognizing the branchpoint at the 3′ splice site of the introns during the early stages of spliceosome assembly (6) and participates in alternative splicing (7, 8). SF3B1 is a core component of U2 and U12 snRNP complexes required for canonical splicing (9). The SPSP motif (S80 and S82) is the main phosphorylation site of SF1 and is targeted by UHMK1 *in vitro*. It has been suggested that phosphorylation of these residues possibly prevents premature association between the SF1–U2AF65 complex and the RNA (10). Despite SF1 and SF3B1 phosphorylation being mediated by UHMK1 and the detection of some pre-mRNA accumulation in the brain of UHMK1 KO mice (11), the direct involvement of this kinase in the splicing process has not been shown so far.

UHMK1 also phosphorylates proteins involved in other cellular processes, such as cell cycle (12), cell migration (13), membrane trafficking (14), local translation in neurons (15),

* For correspondence: Leticia Fröhlich Archangelo, leticiafa@fmrp.usp.br.
Present address for Vanessa C. Arfelli: Laboratory for Experimental Leukemia and Lymphoma Research, Munich University Hospital, Ludwig-Maximilians University (LMU), Munich, Germany.

© 2023 THE AUTHORS. Published by Elsevier Inc on behalf of American Society for Biochemistry and Molecular Biology. This is an open access article under the CC BY-NC-ND license (http://creativecommons.org/licenses/by-nc-nd/4.0/).

and cell differentiation (16, 17). In response to mitogens, UHMK1 is upregulated and phosphorylates the cyclin-dependent kinase inhibitor $p27^{KIP}$ on S10. This phosphorylation leads to $p27^{KIP}$ nuclear export and proteasomal degradation, counteracting the inhibitory effect of $p27^{KIP}$ on the cell cycle (12). Similarly, UHMK1-mediated phosphorylation of Stathmin at S38 targets this protein to degradation, resulting in altered microtubule dynamics and impaired cell migration (13). In neurons and endocrine cells, UHMK1 regulates vesicle secretion through phosphorylation of the Peptidylglycine α-amidating monooxygenase cytosolic domain at S949, which is essential for the correct routing of peptidylglycine α-amidating monooxygenase membranes (18–20). Moreover, it was shown that UHMK1 enhances the local translation of β-actin and AMPA receptors, affecting spine morphology and postsynaptic activity of neurons (15, 21). Additionally, UHMK1 controls the differentiation of osteoclasts and osteoblasts (17) and is upregulated during the differentiation of hematopoietic cells (16). More recently, UHMK1 was associated with cancer-related processes. In hepatocellular cancer, UHMK1 participates in the YAP-UHMK1-MYBL2 (22) and COX5B-UHMK1-ERK (23) axes, contributing to the malignant phenotype by altering the cell cycle and bioenergetics of liver tumor cells, respectively. By reprogramming the nucleotide metabolism through the UHMK1–NCOA3–ATF4 axis, UHMK1 contributes to gastric cancer (24). Also, the involvement of UHMK1 in pancreatic and colon cancers was recently reported (25, 26).

To further characterize the UHMK1 function, we integrated quantitative global phosphoproteomics, RNA-seq, and splicing analysis using the vast-tools pipeline to identify novel putative substrates of this kinase and evaluate UHMK1 participation in gene expression and splicing. We identified a variety of novel UHMK1 candidate substrates that support the role of UHMK1 in biological processes previously associated with this kinase, particularly mRNA splicing. A comprehensive analysis of splicing and functional reporter assay showed for the first time that UHMK1 impacts mRNA splicing *in vivo*. Collectively, our data implicate UHMK1 as a splicing regulatory kinase, connecting protein regulation through phosphorylation and gene expression in key cellular processes.

Results

Global phosphoproteomic analysis revealed a range of putative substrates of the UHMK1 kinase

We performed untargeted quantitative phosphoproteomics of NIH3T3 cells depleted of UHMK1 (shUHMK1#2 and shUHMK1#3) and overexpressing the UHMK1 WT ($UHMK1^{WT}$) and the kinase-dead mutant ($UHMK1^{K54R}$) (Fig. 1, *A* and *B*). We identified a total of 9861 phosphopeptides present in all three replicates of each sample (Table S1), which were filtered by a p-value <0.05 and log2 fold change of $|1|$ to identify differentially phosphorylated phosphopeptides (Fig. 1, *C*–*F*). In shUHMK1#2 and shUHMK1#3 knockdown cells, 12 and 85 phosphopeptides were differentially phosphorylated, respectively, compared to shCTRL control cells. In $UHMK1^{WT}$ and $UHMK1^{K54R}$ overexpressing cells, 53 and 37 phosphopeptides were differentially phosphorylated, respectively, compared to the empty vector (EV) control cells. The 187 differentially phosphorylated phosphopeptides encompassed 163 unique phosphosites within 117 unique differentially phosphorylated proteins (DPPs) (Fig. 1*G*) regarded as UHMK1 putative substrates. Additionally, 25 out of the 187 differentially phosphorylated phosphopeptides contained multiple phosphosites, whereas the remaining 162 phosphopeptides contained single phosphosites (Table S2). Among all phosphosites identified, 91% were serine, 8% threonine, and 1% tyrosine residues (Fig. 1*H*). Of note, 11 phosphosites (Table S2) were not registered in the PHOSIDA and PhosphositePlus databases, suggesting that they are specifically regulated upon UHMK1 modulation, as these phosphosites were not reported in other contexts.

Levels of UHMK1 kinase impact the phosphorylation of the identified substrates

Since virtually all DPPs in shUHMK1#2 were found in shUHMK1#3 cells (Fig. S1), both lists were merged to comprise a total of 69 DPPs in UHMK1 knockdown cells (UHMK1-KD). The DPPs identified in UHMK1-KD and overexpressing cells ($UHMK1^{WT}$ and $UHMK1^{K54R}$) were compared in a Venn diagram (Fig. 2*A*).

Several proteins were differentially phosphorylated exclusively in one condition, *i.e.*, either in UHMK1-KD, $UHMK1^{WT}$, or $UHMK1^{K54R}$. Approximately, 60% of phosphosites within the 52 proteins found exclusively in UHMK1-KD were downregulated, whereas the other 40% were upregulated (Fig. 2*B*). Over 90% of the phosphosites within the 32 DPPs exclusively found in $UHMK1^{WT}$ were upregulated (Fig. 2*C*). Inversely, 80% of the phosphosites within the nine proteins found solely in $UHMK1^{K54R}$ were downregulated (Fig. 2*D*).

Seven proteins, namely Advillin (*Avil*), Predicted gene 7995 (*Gm7995*), Prelamin-A/C (*Lmna*), DNA repair and recombination protein RAD54-like (*Rad54l*), Splicing factor 1 (*Sf1*), Syntaxin-binding protein 4 (*Stxbp4*), and Tubulin polymerization-promoting protein (*Tppp*), were differentially phosphorylated in all conditions (UHMK1-KD, $UHMK1^{WT}$, and $UHMK1^{K54R}$) (Fig. 2*E*). Remarkably, the phosphorylation level of their phosphosites exhibited variable patterns among UHMK1-modulated conditions: the phosphosites Y758 and Y759 of Advillin, S396 of STXBP4, and S80 of GM7995 were upregulated in $UHMK1^{WT}$ and $UHMK1^{K54R}$ cells and downregulated in UHMK1-KD cells. Other phosphosites, such as S404 and S407 of Prelamin-A/C and S182 of TPPP, were upregulated in all conditions. Similarly, the phosphosites T190 and T195 of RAD54-like were upregulated in the majority of the conditions, except in shUHMK1#3. Three phosphopeptides of SF1, a known UHMK1 substrate, were differentially phosphorylated upon UHMK1 modulation. Interestingly, two SF1 peptides comprised exclusively the phosphosite S82, which was downregulated in $UHMK1^{WT}$ and upregulated in UHMK1-KD cells. Both S80 and S82 serines were differentially

ASBMB

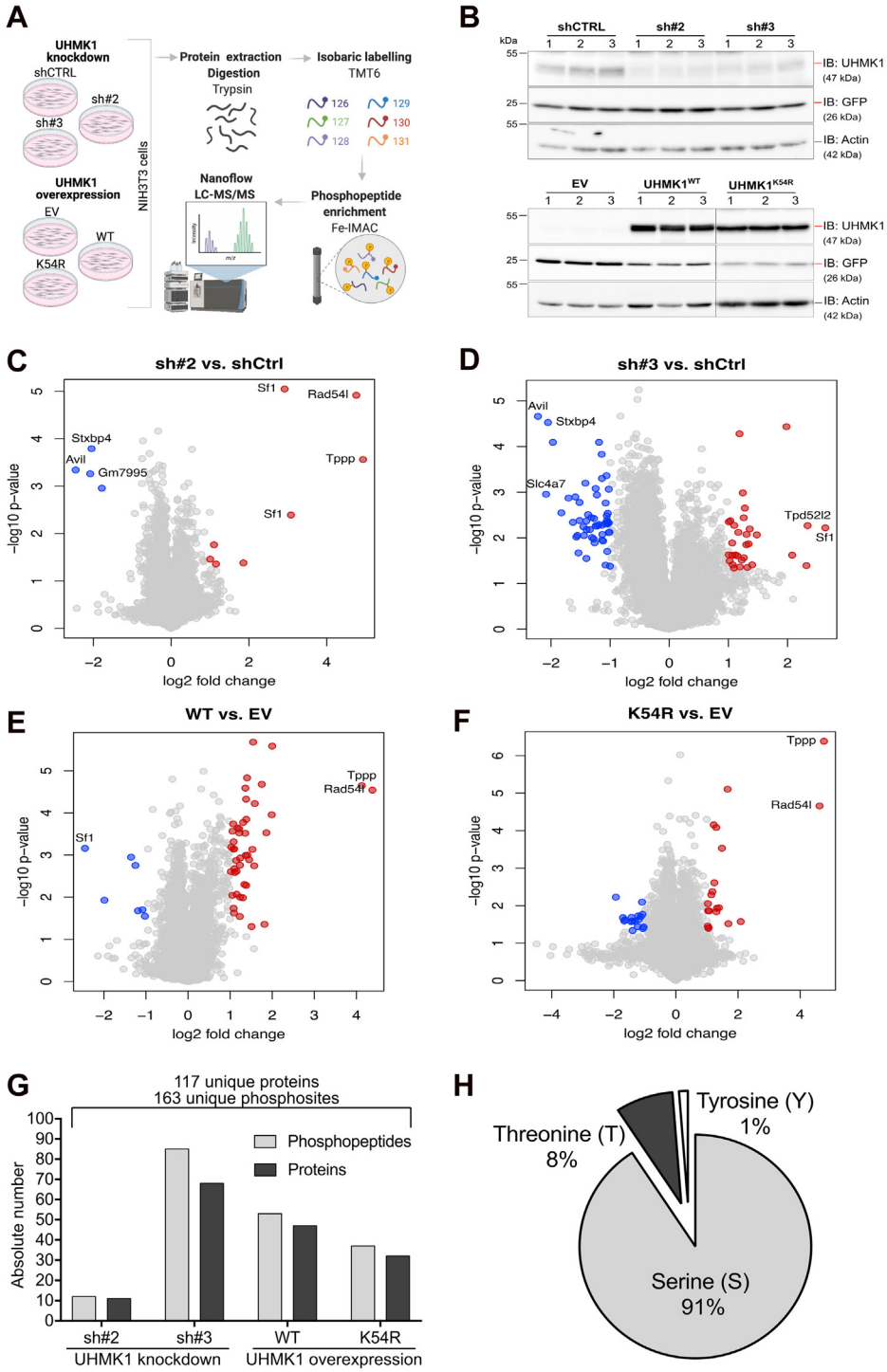

Figure 1. Global impact of UHMK1 on phosphoproteome. *A*, experimental workflow used in the phosphoproteome experiment. UHMK1 modulation in NIH3T3 cells was achieved expressing the shUHMK1#2 (sh#2) and shUHMK1#3 (sh#3) sequences, for knockdown, and UHMK1^{WT} (WT) or the kinase-dead mutant UHMK1^{K54R} (K54R) for overexpression. A scrambled shRNA sequence (shCTRL) and the empty vector (EV) MIY were used as control. Scheme created with ©BioRender.com. *B*, Western blot confirming the efficient modulation of UHMK1 expression in NIH3T3 cells used in the phosphoproteome experiment. The numbers 1 to 3 represent the biological replicates from each condition. Membranes were blotted with anti-UHMK1, anti-GFP, and anti-Actin (loading control). Total protein: 100 μg (knockdown) and 50 μg (overexpression). *C–F*, the volcano plots show the global impact of UHMK1 knockdown (*C* and *D*) and overexpression (*E* and *F*) on phosphoproteome. The *red* and *blue circles* represent the significantly upregulated and downregulated phosphopeptides in each comparison, respectively. Phosphopeptides with *p*-value <0.01 and log2 fold change >|2| have their gene names assigned. *G*, overview of the absolute number of phosphopeptides and corresponding number of proteins differentially phosphorylated in the UHMK1 phosphoproteome. *H*, percentage of phosphorylated Serine, Threonine, and Tyrosine residues in the UHMK1 phosphoproteome. UHMK1, U2AF Homology Motif Kinase 1.

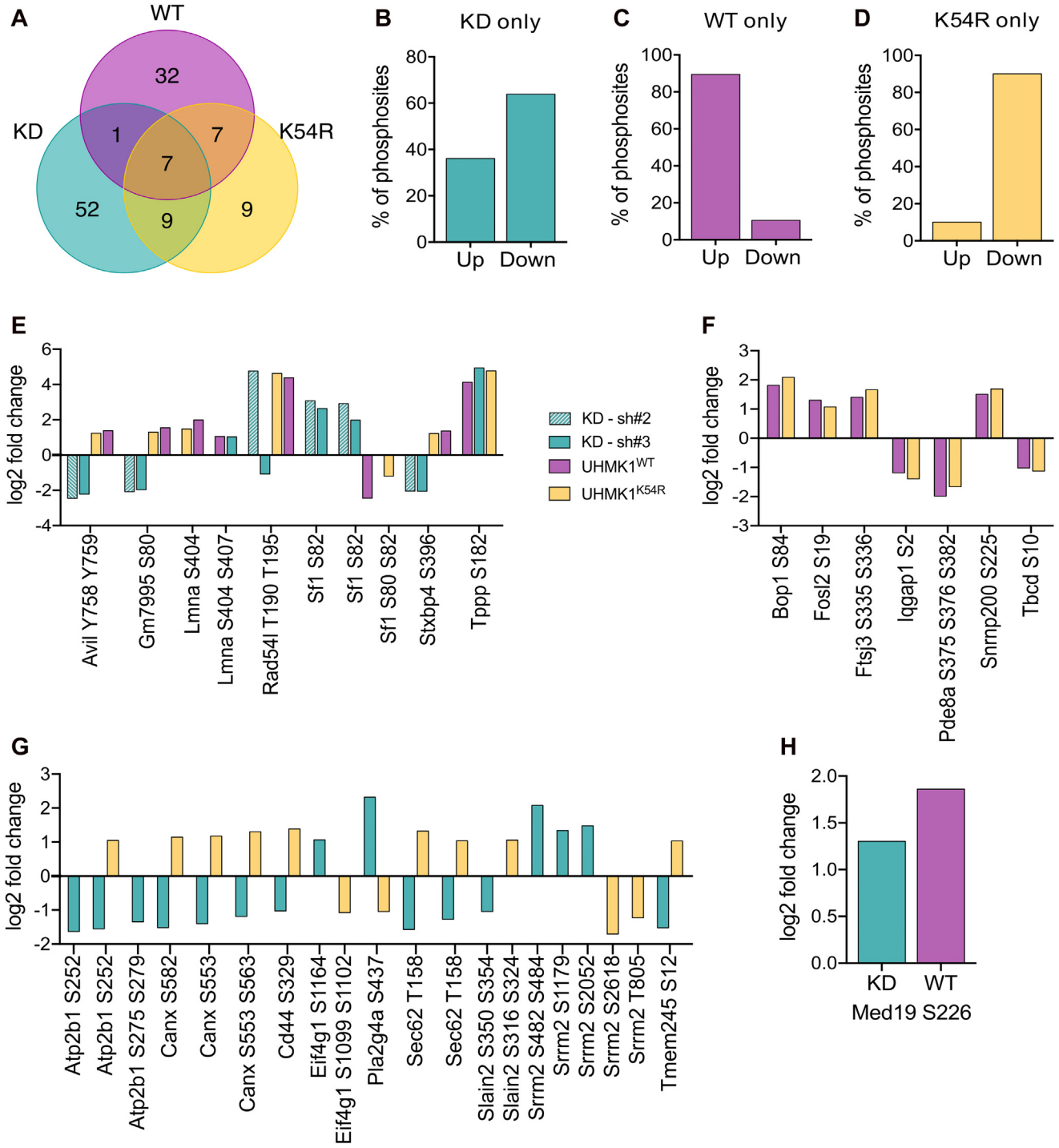

Figure 2. Distribution and phosphorylation pattern of the differentially phosphorylated proteins. *A*, Venn Diagram comparing the number of unique DPPs among the experimental conditions. KD = UHMK1-KD (knockdown); WT = UHMK1^{WT} overexpression; K54R= UHMK1^{K54R} overexpression. *B–D*, percentage of phosphosites upregulated and downregulated in the DPPs found exclusively in UHMK1-KD (*B*), UHMK1^{WT} (*C*), and UHMK1^{K54R} (*D*). *E–H*, phosphorylation pattern of the phosphopeptides (and respective phosphosites) from the DPPs (indicated by their gene names) shared by UHMK1-KD (sh#2 and sh#3), UHMK1^{WT} and UHMK1^{K54R} cells (*E*), UHMK1^{WT} and UHMK1^{K54R} cells (*F*), UHMK1-KD and UHMK1^{K54R} (*G*), and the only DPP (Med19) shared by UHMK1-KD and UHMK1^{WT} (*H*). DPP, differentially phosphorylated protein; UHMK1, U2AF Homology Motif Kinase 1.

phosphorylated (downregulated) in a third phosphopeptide but only in UHMK1^{K54R} cells (Fig. 2*E*).

The phosphosites of the DPPs in both UHMK1^{WT} and UHMK1^{K54R} exhibited the same phosphorylation pattern: either up or downregulated (Fig. 2*F*). Conversely, the phosphosites of the nine proteins regulated in both UHMK1-KD and UHMK1^{K54R} exhibited an opposite phosphorylation pattern in each condition (Fig. 2*G*). The phosphosite S226 of MED19, the only protein regulated in UHMK1-KD and UHMK1^{WT}, was upregulated in both conditions (Fig. 2*H*).

Overall, these results show that UHMK1 overexpression leads to upregulation of the majority of the phosphosites, whereas the expression of the kinase-dead mutant ($UHMK1^{K54R}$) or the UHMK1 knockdown leads to downregulation of most phosphosites. Thus, the phosphorylation pattern of the DPPs is strongly affected by the level of the kinase. Moreover, the data point to a dynamic and complex regulation of the differentially phosphorylated substrates present in more than one condition, some of which might be indirectly regulated by UHMK1.

UHMK1 preferentially phosphorylates proline-directed residues surrounded by charged amino acids

UHMK1 preferentially phosphorylates proline-directed serine residues *in vitro* (2). We therefore sought to evaluate whether the same phosphorylation preference was present in our data. For these analyses, we considered the most likely direct targets of UHMK1, *i.e.*, proteins whose phosphosites were upregulated in $UHMK1^{WT}$ and downregulated in UHMK1-KD. Additionally, we included all the phosphosites regulated in $UHMK1^{K54R}$, since many of these phosphosites were downregulated in this condition, having a similar effect of UHMK1-KD (Fig. 2*D*) or presented a pattern similar to $UHMK1^{WT}$ (possibly due to residual endogenous activity Fig. 2, *F* and *G*). Using the software pLogo for motif search (27), we confirmed phospho-serines (S) followed by proline (P) at position +1 with high frequency (41.67%) and statistical significance (Fig. 3*A*). Besides, glutamic acid (E) was present at positions −4 (17.71%), +2 (18.75%), and +3 (20.83%), while arginine (R) was common at position −3 in 16.67% of the phosphosites analyzed. These residues have the common feature of being charged (R = positively charged; E = negatively charged). As in our data the ERXXSPEE consensus sequence was not present in single phosphopeptides, this result indicates a preference of UHMK1 for these residues or, more generally, charged amino acids in these specific positions *in vivo*. However, the presence of the whole sequence is not a requirement for the phosphorylation of the serine residues. Additionally, UHMK1 also significantly phosphorylated proline-directed threonines (Fig. 3*B*). However, the limited number of phospho-threonines matching the criteria used for this analysis (n = 5) did not allow the identification of a broader consensus sequence. In summary, our data confirm UHMK1 as a preferential proline-directed kinase in a considerable number of substrates as recently described (28), with a preference for charged amino acids surrounding the targeted serine residues.

UHMK1 putative substrates are mainly implicated in RNA processing

To better understand the UHMK1 function, we performed a Gene Ontology (GO) enrichment analysis with the 117 DPPs regulated upon UHMK1 modulation. Among the Biological Process (BP) terms identified are "mRNA splicing *via* spliceosome", "cell division", "microtubule cytoskeleton organization", "positive regulation of protein localization to cell periphery", "translational initiation", and "maturation of LSU-rRNA from tricistronic rRNA transcript" (Fig. 4*A*). Moreover, the terms "heterocyclic/aromatic compound metabolic process" and "nitrogen metabolic process" (and their related terms) recurrently appeared (Table S3). In addition, Reactome pathway analysis identified the pathways "eukaryotic translation elongation" (FDR = 0.00249) and "mRNA splicing – major pathway" (FDR = 0.00112) as statistically significant (not shown). The GO analysis confirmed the UHMK1 function in some cellular processes previously reported (cell cycle, microtubule cytoskeleton organization, translation, protein transport to the cell periphery) and previously suggested (mRNA splicing, cell division, nitrogen/aromatic compound metabolic process), as well as in a novel function, namely in rRNA processing.

The interaction network of UHMK1 and the 117 putative substrates (DPPs) was accessed using the STRING database (Fig. 4*B*). Proteins annotated in some of the BP terms retrieved from the GO analysis were identified as interaction clusters, from which the most prominent comprised the splicing regulatory proteins SF1, SNRNP200, hnRNP M (*Hnrnpm*), SRSF2, USP39, SRRM2, PRPF38A, SRSF4, and SUGP1, together with PRPF4B, PRPF38B, LUC7L, THRAP3, PPP4R2, and SON, which were presented as intercluster interactions. Of note, the kinases AHNAK and PRPF4B and the phosphatase PPP4R2 interact with proteins within this cluster, indicating an additional layer of regulation, whereby UHMK1 could affect the phosphorylation of these targets. Moreover, there were marked intracluster and intercluster interactions evident among translation factors: EF-2 (*Eef2*), EF-1-delta (*Eef1d*), EF-1-gamma (*Eef1g*), ABCF1, eIF-2-beta (*Eif2s2*), eIF-2B subunit epsilon (*Eif2b5*), eIF-4-gamma 1 (*Eif4g1*), and eIF4E-binding protein 1 (*Eif4ebp1*). Yet, the proteins involved in rRNA processing (BOP1, MPP10 (*Mphosph10*), FTSJ3, and NPM1) and proteins that act in synaptic vesicles (PGRMC1, DNAJC5, SNAP23, STX4A, and STXBP4) formed two other additional clusters of interacting proteins. Interestingly, proteins related to cell cycle and cell division do not form an obvious interacting cluster but are also frequently associated with microtubule cytoskeleton organization (NUMA1, SON, Stathmin (*Stmn1*), and MAP4) (Fig. 4*B*). In summary, our data demonstrate that UHMK1 regulates a large number of intrinsically connected RNA-related proteins. The most statistically significant RNA-related proteins regulated in UHMK1 overexpression, namely SF1 and SUGP1, were validated as direct substrates of UHMK1 in follow-up experiments (Fig. S2, *A* and *C*).

A subset of the RNA-related UHMK1 substrates contain putative ULM motifs

Since UHM domains are known to interact with UHM-ligand motif (ULM) of splicing factors (3), we searched for putative ULM motifs within the amino acid sequences of the 28 RNA-related DPPs annotated in the RNA-related BP terms of the GO analysis plus an additional protein known from the literature to be involved in splicing regulation (29). Search of the [RK]- X(0,3)-W- [DN]- [EQ] ULM pattern (30) in ScanProsite returned two proteins owning *bona fide* ULM motif: SF1, whose

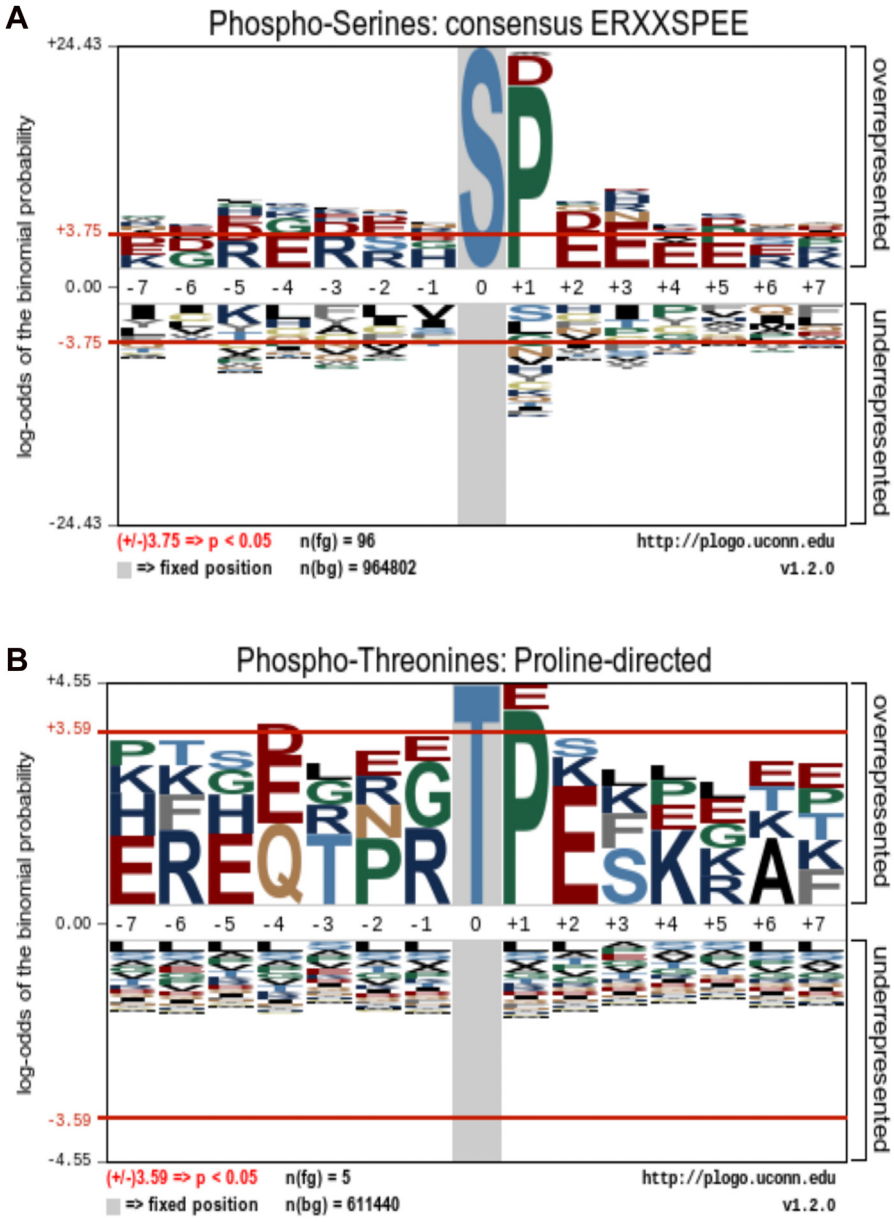

Figure 3. UHMK1 phosphorylation consensus sequence retrieved from pLogo analysis. Amino acid heights are scaled according to their statistical significance, as well as the stacking order (the most significant residues are positioned closest to the x axis). The *red horizontal lines* represent a threshold for Bonferroni-corrected statistical significance values. Positive values higher than the threshold correspond to statistically significant ($p < 0.05$) over-represented amino acids. Negative values lower than the threshold correspond to statistically significant underrepresented amino acids. *A*, UHMK1 preferentially phosphorylates proline-directed serine within the consensus sequence ERXXSPEE. Input sequences = 96. Log-odds of the binomial probability: E (−4) = 3.89; R (−3) = 3.81; P (+1) = 20.32; E (+2) = 4.36; E (+3) = 5.07. *B*, proline-directed threonine is also preferentially phosphorylated by UHMK1. Input sequences = 5. P (+1) = 4.03. UHMK1, U2AF Homology Motif Kinase 1.

ULM motif has been extensively characterized (5), and the RNA helicase TNRCB6. Since the ULM motif is highly degenerate and variations to the previously reported pattern may exist (30), we further investigated the putative ULM motifs in the 29 RNA/splicing-related proteins based on protein alignment. We first considered candidates for the alignment proteins bearing the conserved tryptophan (W) and at least two amino acids in assigned positions from the established ULM pattern. Those candidates were aligned with well-characterized ULM motifs from four other factors ($U2AF^{65}$, SF3B1, ATX1, MAN1 (30)). Using this approach, we identified 12 proteins with putative ULM motifs. Therefore, in addition to SF1 and SUGP1 (31), 10 out of the 29 RNA/splicing-related DPPs (SNRNP200, THRAP3, SAFB, PRPF38A, USP39, FTSJ3, ZNF638, SETD2, EEF1D, and TNR6CB) contain putative ULM domains (Fig. 5) and are likely potential candidates for direct interaction with UHMK1. In fact, coimmunoprecipitation experiments revealed a clear interaction of SUGP1 with UHMK1, which is partly dependent on the UHM domain of UHMK1 (Fig. S2*B*).

UHMK1 modulation impacts alternative splicing

Because several UHMK1 putative substrates are mainly related to mRNA splicing (Fig. 4), we submitted $UHMK1^{WT}$ and UHMK1-KD cells (Fig. S3) to RNA-seq and investigated

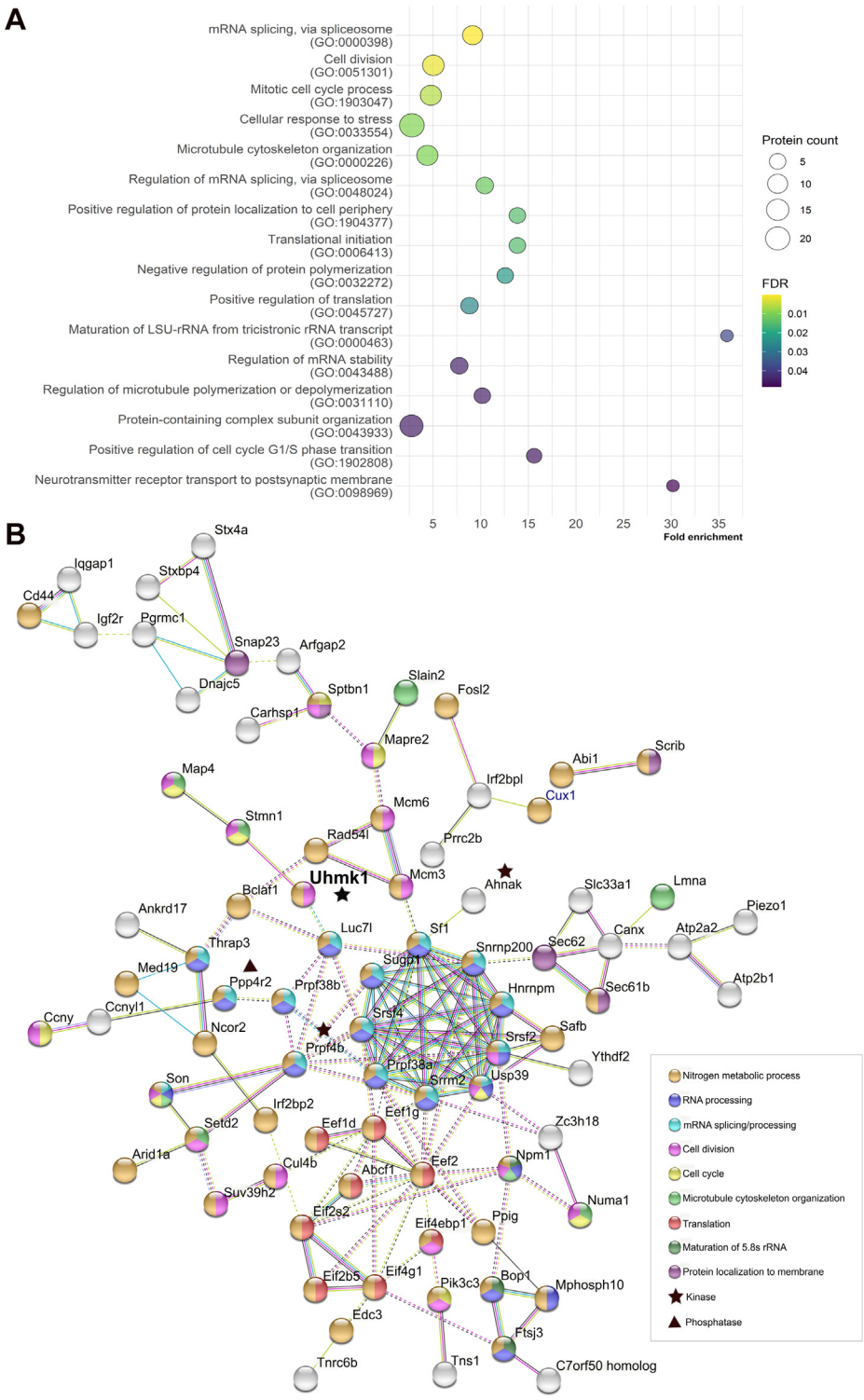

Figure 4. UHMK1 putative substrates are implicated in a variety of cellular processes and form a complex network. *A*, Biological Process (BP) terms retrieved from Gene Ontology (GO) analysis. Only the most specific terms within the hierarchy presented in PANTHER are shown (complete results in Table S3, specific terms highlighted in *gray*). *B*, interaction network of UHMK1 and the 117 putative substrates (DPPs). Only the interacting proteins (represented by their gene names) are shown in the figure: the *pink* edges represent the experimentally determined interactions; *blue* edges represent interactions registered in curated databases; *green* edges represent interactions extracted from text mining; *black* edges represent coexpression. Each node represents one protein. Node colors indicate the most representative BP terms from GO analysis. Intercluster interactions are represented by *dashed edges*. Protein-protein interaction (PPI) enrichment *p*-value: 4.55e-15. The kinases and the phosphatase in this network are marked with a *black star* and a *triangle*, respectively. UHMK1 is highlighted in *bold*. DPP, differentially phosphorylated protein; UHMK1, U2AF Homology Motif Kinase 1.

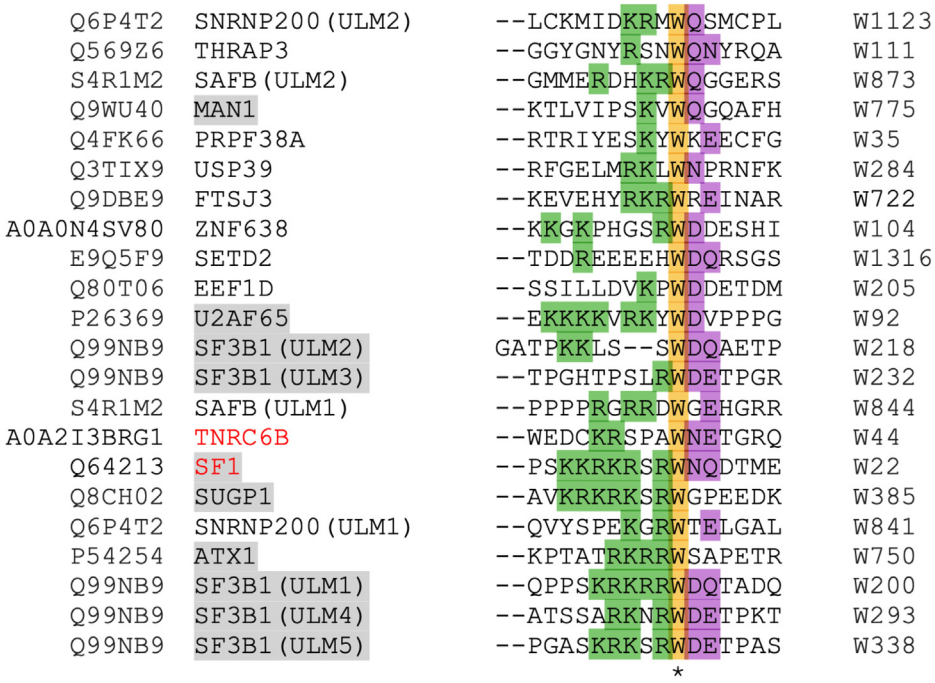

Figure 5. Besides SF1 and SUGP1, 10 RNA/splicing-related DPPs contain ULM motifs. Clustal Omega alignment of proteins containing well characterized ULM motifs (highlighted in *gray*) and the ten novel RNA/splicing-related putative UHMK1 substrates. Uniprot identification code for the mouse proteins are shown (*left*). The conserved tryptophan (W) within the ULM domain is highlighted in *yellow*, and its position within the protein is depicted on the *right*. The preferred amino acids in the positions +1 and +2 are highlighted in *purple*, and the preferred amino acids at −1 and previous positions are highlighted in *green*. TNRC6B and SF1 (*red*) were the only RNA-related proteins from our study considered as *bona fide* ULM-containing proteins in ScanProsite analysis (not shown). DPP, differentially phosphorylated protein; UHMK1, U2AF Homology Motif Kinase 1; ULM, UHM ligand motif.

alternative splicing events (ASEs). A total of 179 statistically significant differentially spliced events were identified upon UHMK1 knockdown (Fig. 6*A*) and 97 upon UHMK1^{WT} overexpression (Fig. 6*B*). Overall, the most common type of event observed was the inclusion/exclusion of cassette exons, with 115 events (64%) occurring in UHMK1 knockdown and 51 events (52%) occurring after UHMK1^{WT} overexpression. Alternative 3′ splice sites (acceptor sites) and 5′ splice sites (donor sites) had a smaller sampling, with a total of 64 events (36%) in UHMK1 knockdown and 46 events (47%) in UHMK1^{WT} overexpression. No intronic events were observed in the conditions analyzed. Among all ASEs identified, 12 events were shared between UHMK1 overexpression and knockdown (Fig. S4*A*), four of them (Dcun1d5:MmuALTD0004036-4/6, Cpsf6:MmuALTA0004602-4/4, Cpsf6:MmuALTA0004602-3/4, Cdca2:MmuALTA0003700-1/2) were altered in the same direction (included/excluded) in both experimental conditions, while the remaining eight events (Upk3bl:MmuALTA0000280-1/2, Upk3bl:MmuALTA0000280-2/2, Ktn1:MmuEX0025964, Mrps33:MmuALTD0008795-1/2, Mrps33:MmuALTD0008795-2/2, Insig2:MmuEX0024241, Safb2:MmuEX0040926, Kif20b:MmuEX0025516) were altered in opposite directions.

Analysis of the predicted impact of the ASEs on coding sequences revealed that 53% (95 events) of ASEs in UHMK1 knockdown cells mainly predicted alternative isoforms with neutral impact, whereas 12% (22 events) exhibited a disruptive, and 21% (39 events) a protective impact on the ORF of the proteins they encode (Fig. 6*C*). In UHMK1^{WT} overexpressing cells, 54% (53 events) of the splicing changes were predicted as alternative isoform (neutral), 16% (16 events) were predicted to disrupt the ORF, and 14% (14 events) predicted a protective function (Fig. 6*D*). The percent spliced in (PSI) of the 20 most significant cassette exons are depicted in Figure. 6, *E* and *F*. Among those, disruptive ASEs were found in the transcripts of *Safb2*, *Mllt10*, and *Ktn1* (UHMK1 knockdown) and *Usp16*, *Ptpn11*, *Scfd1*, and *Dtnb* (UHMK1^{WT}). Interestingly, GO analysis of the list of genes exhibiting ASEs in UHMK1 knockdown returned BP terms mainly related to cell-cycle, microtubule organization, and metabolic process (Fig. S4*B*), which were also found in the GO analysis of the UHMK1 phosphoproteome (Fig. 4).

To further explore the contributions of UHMK1 to splicing regulation, we performed an *in vivo* splicing reporter assay. HEK 293T cells were transfected with the reporter plasmid and UHMK1^{WT} or UHMK1^{K54R} alone and in combination with the UHMK1 substrate, SF1. Expression of UHMK1^{WT} alone increased the activity of the reporter only by 10% over the control (EV MIY), whereas splicing activity was barely observed upon expression of the UHMK1 kinase dead-mutant (−6% compared to the control) (Fig. 6*G*). To evaluate the impact of UHMK1 on SF1-mediated splicing, UHMK1 was coexpressed with SF1 and the reporter plasmid. Expression of SF1 alone enhanced the activity of the reporter by 41% over the control (EV pcDNA). Coexpression of UHMK1^{WT} enhanced SF1 function on the splicing of the reporter gene by 18% compared to SF1 alone. The effect of UHMK1 on SF1 was dependent on the kinase activity since expression of the UHMK1^{K54R} did not enhance SF1-mediated splicing (−25%

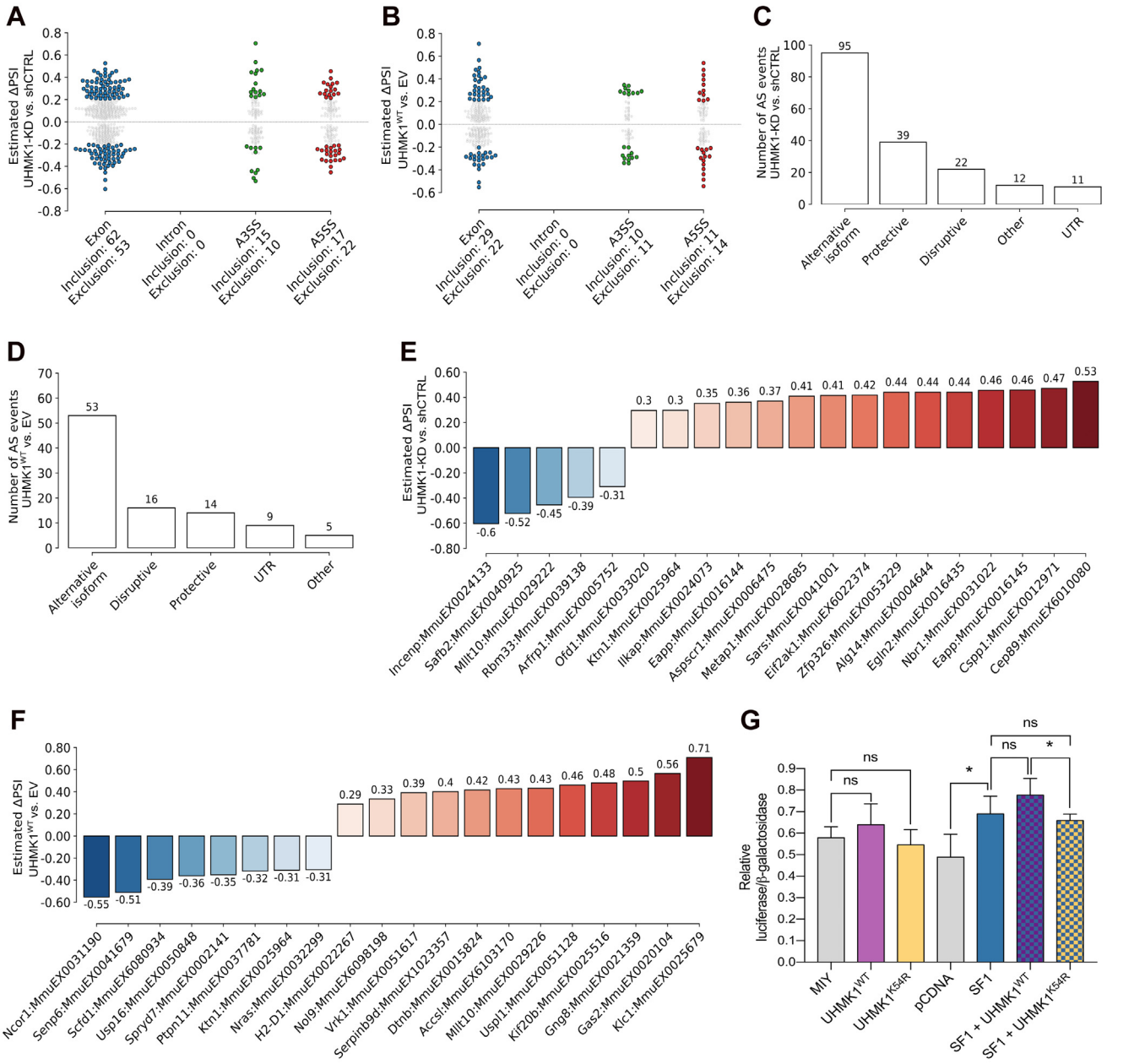

Figure 6. UHMK1 impacts mRNA splicing. *A–F*, splicing analysis from UHMK1 RNA-seq data, comparing UHMK1 knockdown (UHMK1-KD) with shCTRL cells and UHMK1^{WT} overexpressing cells with the empty vector (EV) control cells. *A* and *B*, significant alternative splicing events (ASEs) in UHMK1-KD and UHMK1^{WT} overexpressing cells, respectively; *C* and *D*, predicted impact on coding sequence by ASE; *E* and *F*, percent spliced in (PSI) levels for the top 20 most significant Exon inclusion/exclusion ASEs. *G*, splicing reporter assay. The ratio between β-galactosidase and luciferase is an indirect measure of splicing occurring between both genes. Average values of four independent experiments. Constant amount of the pTN24 reporter plasmid is present in all conditions. One way ANOVA followed by Bonferroni correction was used to compare UHMK1^{WT} and UHMK1^{K54R} to the empty vector control MIY (not significant). Increase in splicing in SF1 over pcDNA (p = 0.0244) and difference between SF1+UHMK1^{WT} and SF1+UHMK1^{K54R} (p = 0.0294) was confirmed by Student t test. Controls of gene expression levels of UHMK1 and SF1 are provided in Fig. S5. UHMK1, U2AF Homology Motif Kinase 1.

compared to SF1+UHMK1^{WT}, p = 0.0294). Although the differences were subtle, they were consistently observed in four independent experiments. Levels of *UHMK1* and *SF1* expression are shown in Fig. S5. Taken together, our data show for the first time that UHMK1 modulation can impact splicing and implicate UHMK1 as a regulatory splicing kinase.

UHMK1 modestly impacts transcript expression levels

Since splicing and gene expression are tightly coordinated processes (32), we sought to evaluate the UHMK1 impact on transcript expression levels by RNA-seq. Differential expression analysis revealed that modulation of UHMK1 had a modest impact on global transcript expression levels, as observed in the Principal Component Analysis plots (Fig. 7, *A* and *B*). UHMK1 knockdown (UHMK1-KD), mediated by the expression of shUHMK1#1, shUHMK1#2, and shUHMK1#3 sequences, altered the expression of 32 genes, of which 17 were upregulated and 15 were downregulated (Fig. 7, *C* and *D*, and Table S4). UHMK1^{WT} overexpression did not affect transcript expression levels, as *Uhmk1* was the only

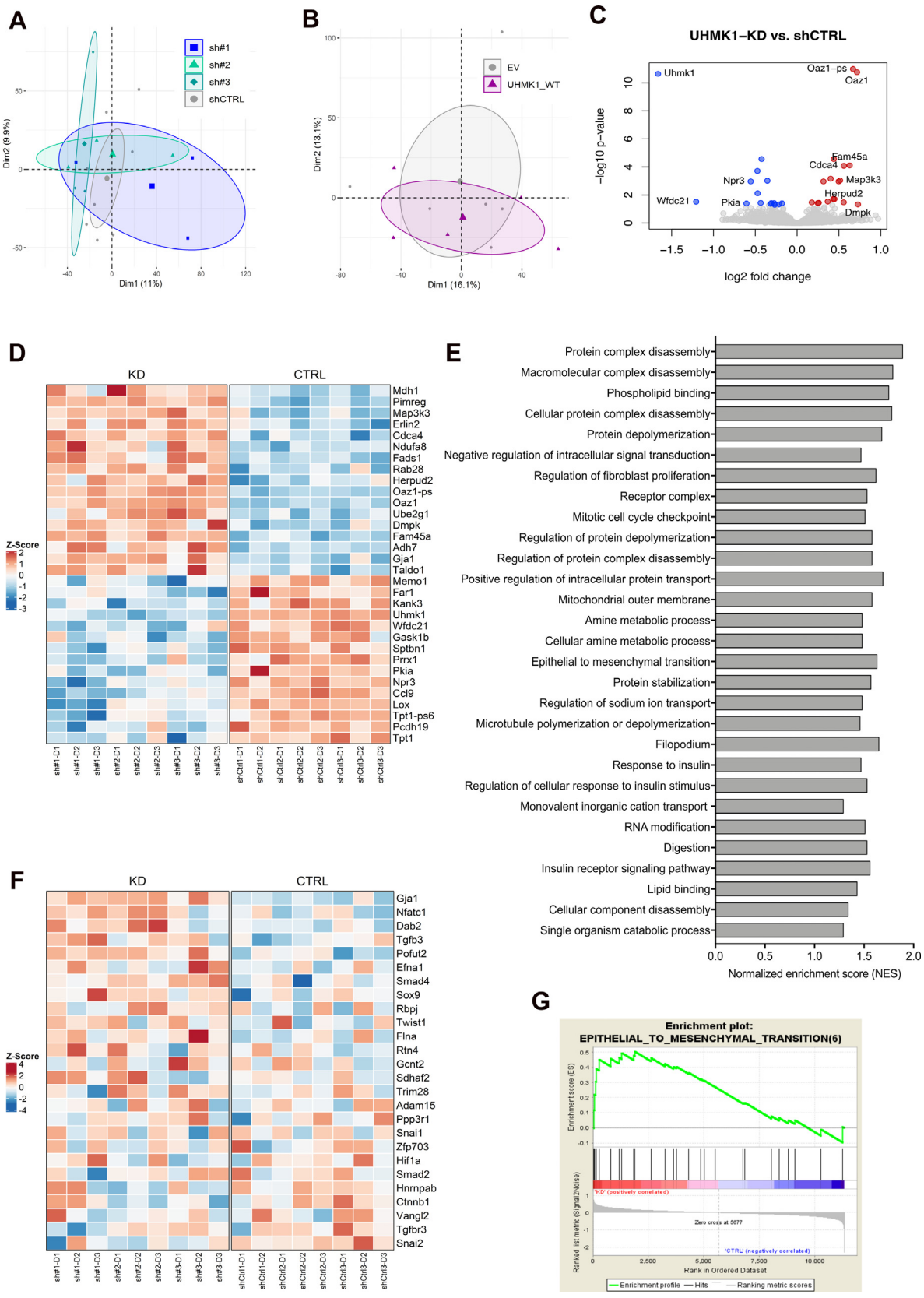

Figure 7. UHMK1 impacts gene expression. *A* and *B*, Principal Component Analysis (PCA) plots showing the overall effect of UHMK1 knockdown mediated by shUHMK1#1 (sh#1), shUHMK1#2 (sh#2), and shUHMK1#3 (sh#3) compared to shCTRL and UHMK1^{WT} overexpression compared to empty vector (EV) control, respectively. *C*, volcano plot showing the differentially expressed genes (DEGs) in UHMK1-KD cells (shUHMK1#1, shUHMK1#2, and shUHMK1#3 combined as one single artificial condition) compared to shCTRL cells. *p*-value <0.05 was used as cutoff. Genes with log2 fold change $>|0.5|$ are labeled. *D*, heatmap of expression of the 32 DEGs represented as z-score of normalized counts, in each replicate of UHMK1 knockdown (KD) and shCTRL (CTRL) cells. *E*, gene sets enriched in UHMK1-KD in GSEA analysis. *F*, heatmap showing the expression of the Epithelial Mesenchymal Transition (EMT)-enriched gene set in UHMK1 knockdown cells. Gene expression is represented as z-score of normalized counts. *G*, enrichment plot for EMT gene signature. GSEA, Gene Set Enrichment Analysis; UHMK1, U2AF Homology Motif Kinase 1.

differentially expressed gene in this setting (data not shown). Although UHMK1 knockdown had a small impact on transcript expression, with log2 fold changes <|2| (Table S4), we validated these findings by a quantitative PCR (qPCR) array of selected targets in an independent transduction experiment of NIH3T3 cells (Fig. S6).

GSEA analysis implicates UHMK1 in epithelial-mesenchymal transition

Gene Set Enrichment Analysis (GSEA) revealed 29 enriched gene sets in UHMK1 knockdown cells, considering a nominal *p*-value <0.05 (Fig. 7*E*). Although none of the gene sets crossed the 25% false discovery rate (FDR) threshold (<0.25), 4 out of 29 were related to functions previously associated with UHMK1 in the literature, namely "regulation of fibroblast proliferation" and "mitotic cell cycle checkpoint"; "microtubule polymerization or depolymerization", and "RNA modification". Moreover, these four gene sets were also observed as related terms in GO analysis of the UHMK1-regulated proteins (Fig. 4 and Table S3). Therefore, it is plausible that the 29 enriched gene sets are true UHMK1-related pathways. Among the enriched gene sets, epithelial-mesenchymal transition (EMT) showed the highest percentage of genes with dichotomized expression pattern between UHMK1 knockdown and control samples (Fig. 7, *F* and *G*) suggesting that UHMK1 may play a role in EMT.

UHMK1 affects proliferation, clonogenicity, and migration of NIH3T3 cells

Because the GO and GSEA analysis returned terms related to cell cycle, cell division, and migration, we performed functional assays with UHMK1 overexpressing and knockdown NIH3T3 cells to evaluate the phenotypes related to those cellular processes (Fig. 8).

Proliferation was significantly reduced in UHMK1 knockdown cells (shUHMK1#1 and shUHMK1#2), whereas in $UHMK1^{WT}$ overexpressing cells, there were no effects on proliferation (Fig. 8*A*). In colony-forming assay, no difference in the percentage of colonies formed was observed with shUHMK1#1, shUHMK1#2, or shUHMK1#3 cells compared to shCTRL cells, while $UHMK1^{WT}$ overexpressing cells formed 20% less colonies than control cells (Fig. 8*B*). Viability and apoptosis were also not affected upon UHMK1 modulation (Fig. 8, *C* and *D*).

Finally, transwell chemotaxis assay revealed that UHMK1 knockdown cells migrated less than shCTRL cells (Fig. 8*E* left panel and Figs. S7 and S8). Conversely, $UHMK1^{WT}$ overexpression increased migration of cells towards the gradient, whereas overexpression of the UHMK1 kinase-dead mutant ($UHMK1^{K54R}$) had no effect on cell migration and was comparable to control cells (Fig. 8*E* right panel and Figs. S7 and S9).

Discussion

The implication of UHMK1 function in cellular processes such as cell cycle, migration, membrane trafficking, local translation in neurons, and mRNA metabolism is mainly based on the knowledge of the UHMK1 interaction with particular binding partners involved in these processes (4, 12, 13, 15, 20). To our knowledge, this study is the first large-scale investigation of the UHMK1 phosphoproteome, carried out using UHMK1-depleted and UHMK1-overexpressing cells.

Our phosphoproteome results showed that UHMK1 regulates phosphosites of 117 proteins, of which 106 are novel putative substrates for the kinase. The fact that 10% of the proteins identified are either known UHMK1 substrates, such as SF1 (4), Stathmin (13, 33), and NPM1 (23), or have been previously described as potential UHMK1-interacting proteins, such as STXBP4, TNRC6B, IRF2BP2, NCOR2, YTHDF2, SUGP1, hnRNP M, and PRRC2B (22), points to the accuracy of our findings. Even though some of the UHMK1 known substrates did not appear in this initial screen, for instance, SF3B1 (5), $p27^{KIP}$ (12), and PIMREG (34), they were identified in one or other experimental conditions below the cutoff employed, further confirming the stringency of the study. Of note, five kinases (PIK3C3, WNK1, NUCKS1, PRPF4B, and AHNAK) and two phosphatases (PPP4R2 and PTPN21) were found among the UHMK1 putative substrates. These proteins likely contribute to additional layers of regulation of the DPPs, some of which might be only indirectly regulated by UHMK1, through these kinases and phosphatases.

GO enrichment analysis of the 117 putative substrates confirmed UHMK1 function in cellular processes previously associated with this kinase (mRNA splicing (4), cell cycle (12); cytoskeleton (microtubule) organization (13); translation (15, 21), membrane trafficking (19, 20), and nucleotide metabolism (24)) and pointed to a novel function of UHMK1 in rRNA processing. Most importantly, our data broadened the knowledge of the protein network and the players regulated by UHMK1 in each of these processes. Moreover, the fact that many of the UHMK1 putative substrates interact with each other and between the clusters (Fig. 4*B*) indicates that UHMK1 is important for regulating complex networks of proteins that coordinate diverse (and yet complementary) biological processes in the cell.

Remarkably, 24% of the putative UHMK1 substrates are RNA-related proteins and the most prominent interaction network in STRING analysis is comprised of splicing regulatory factors, followed by translation factors and rRNA processing proteins. A closer look at the function of the most prominent group revealed that most of the proteins are involved in the spliceosome, at the complexes E, A, and B, but also in the further steps of the splicing cycle (Fig. 9). It is well known that the phosphorylation status of splicing factors impacts the assembly of the spliceosome, as it affects interaction among them and with the mRNA. Moreover, phosphorylation controls the intracellular and intranuclear localization of splicing factors, altering their concentration and consequently splice site selection (35). Two major families of splicing regulatory kinases, namely the SRPKs and CLKs, are responsible for phosphorylating splicing factors (36). This is the first report describing UHMK1 as a broad splicing regulatory kinase. However, the consequences of the UHMK1-mediated

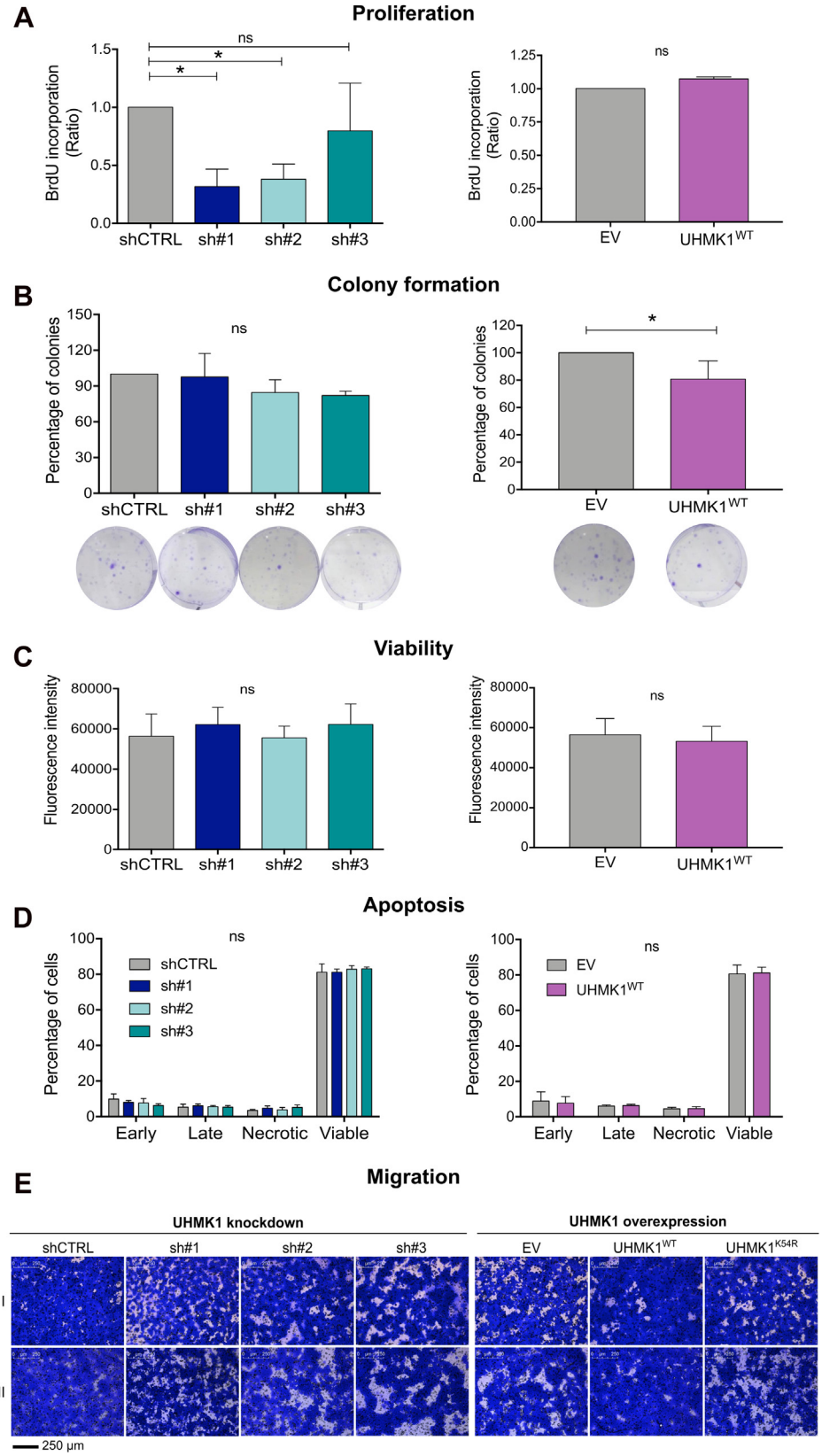

Figure 8. UHMK1 affects proliferation, colony formation, and migration of NIH3T3 cells. *A*, proliferation was evaluated by the percentage of cells that incorporated BrdU. Charts represent the ratio of BrdU incorporation in UHMK1 knockdown mediated by shUHMK1#1 (sh#1), shUHMK1#2 (sh#2), and shUHMK1#3 (sh#3) relative to the scrambled control (shCTRL) cells and UHMK1^{WT} overexpressing cells relative to empty vector (EV) cells. Data from three independent experiments (*$p < 0.05$, One-way ANOVA followed by Bonferroni's multiple comparison test). *B*, clonogenic assay. The bar plots represent the percentage of colonies in UHMK1 knockdown and UHMK1^{WT} overexpressing cells relative to the shCTRL or empty vector (EV), respectively. Results from three independent experiments, carried out in triplicate (*$p = 0.0286$, Mann-Whitney test). The representative images of crystal *violet*-stained colonies are

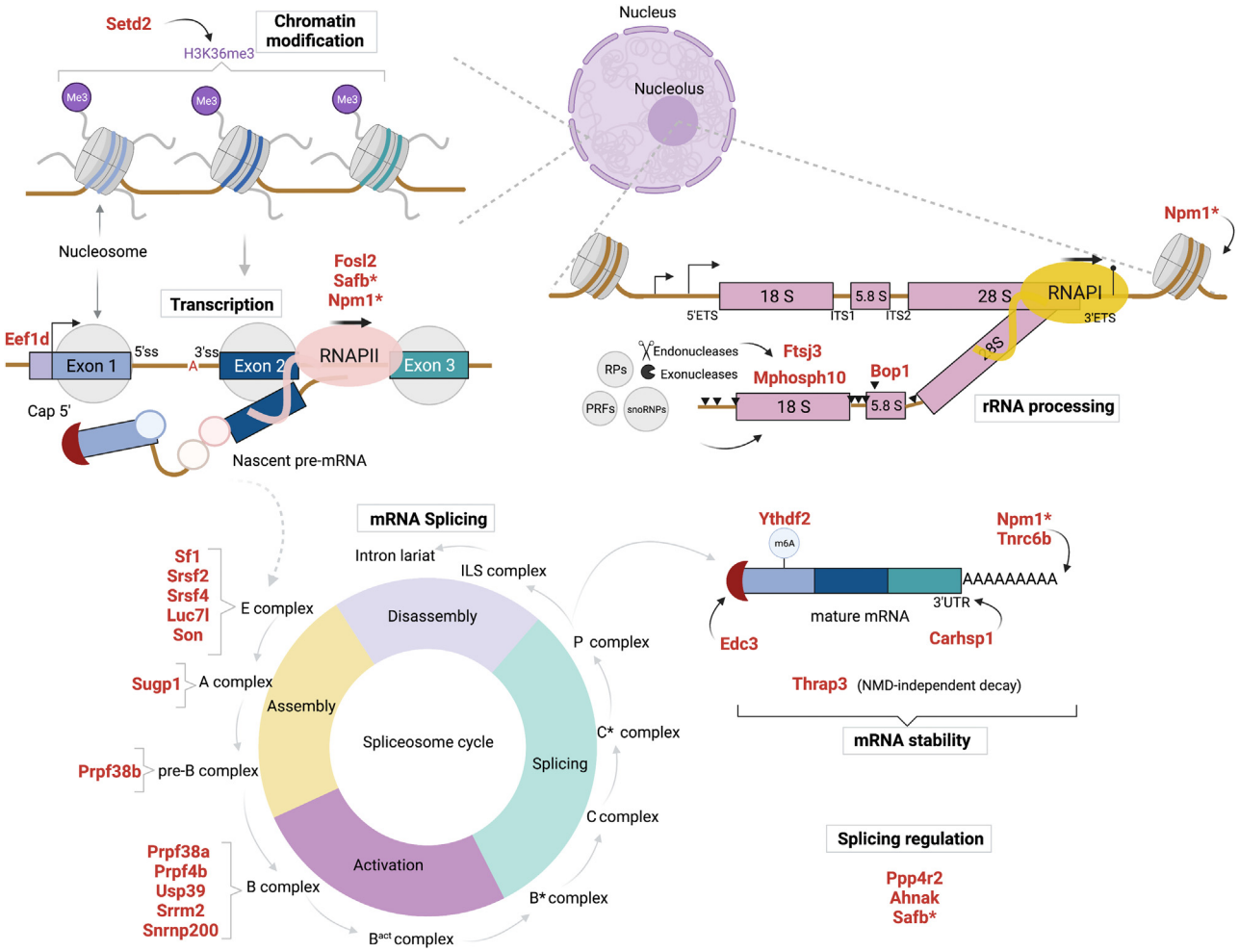

Figure 9. Schematic view of the role of the 28 RNA-related UHMK1 substrates (DPPs) in different layers of gene expression. We searched the role of the 28 RNA-related DPPs in the literature, UniProt (90) and Spliceosome (91) databases. The RNA-related DPPs are represented by their gene names and highlighted in *red*. Proteins that act in more than one function related to RNA metabolism are marked with an asterisk (*). The main functions are highlighted in a *box*: Chromatin modification, Transcription, mRNA splicing, Splicing regulation, mRNA stability, and rRNA processing. Approximately, half of the novel RNA-related UHMK1 substrates (15 proteins) are components of the spliceosome. Six DPPs have a role in mRNA stability, through mechanisms involving the poly(A) tail (TNRC6B (92) and NPM1 (93)), the 5′ Cap (EDC3 (94)), binding to N6-methyladenosine mRNAs (YTHDF2 (95)), nonsense-mediated decay (NMD)-independent decay (THRAP3 (96)), and binding to 3′ UTR (CRHSP-24 - *Carhsp1*) (97)). Four of the RNA-related DPPs act in transcription, either by acting on RNA pol II regulation (SAFB (98) and NPM1 (99)) or as transcription factors (FRA-2 - *Fosl2*) (100) and Eef1d (101)). SETD2, a methyltransferase responsible for H3K36me3 mark, act in chromatin modification (102). Moreover, three DPPs act specifically in the cleavage of the tricistronic rRNA transcript: MPP10 (*Mphosph10*) (component of the U3 snoRNP) and FTSJ3 (2′-O-methyltransferase) are involved in the processing of the 18S rRNA (103, 104), while BOP1 (component of the PeBoW complex) is necessary for the processing of 5.8S and 28S rRNAs (105). NPM1 also acts in the nucleolus as a histone chaperone, affecting chromatin status of rDNA (99). Created with ©BioRender.com. DPP, differentially phosphorylated protein; PRFs, preribosomal factors; RPs, ribosomal proteins; UHMK1, U2AF Homology Motif Kinase 1.

regulation of the phosphosites of these proteins remain to be investigated.

Splicing analysis of transcriptome data revealed that UHMK1 modulation affected over 270 ASEs, most of which led to exon inclusion/exclusion and produced alternative isoforms. Since our analysis was performed on Prime-seq data (37) and the reads were sequenced mainly from the 3′ end of the transcripts, one limitation of our analysis is that we only evaluated ASEs occurring within this region of the transcripts. Thus, we cannot consider it a global splicing analysis as the identified ASEs are likely to be underrepresented. Nonetheless, our data is a proof-of-principle that UHMK1 affects alternative

shown. One colony was defined by the minimum of 50 cells. *C*, viability assay. For UHMK1 knockdown cells, the chart represents the average of four experiments performed in sextuplicate. For UHMK1^{WT} overexpressing cells, the chart represents the average of five experiments, two performed in triplicate and three performed in sextuplicate. *D*, apoptosis evaluation by Annexin V assay. Mean from three independent experiments. Early apoptosis is defined by the cells that are positive only for Annexin V; late apoptosis comprises the cells that are positive for both Annexin V and propidium iodide (PI); Necrotic cells are positive only for PI and Viable cells are negative for both markers. *E*, migration assay. Representative images of two independent experiments (I and II) with UHMK1 knockdown and UHMK1^{WT} overexpressing cells. The experiments were performed in duplicates. Three images from each replicate were taken: in the *center*, *bottom*, and *top* of the membrane, relative to position of the circumference in the plate. The images in this figure are representative of the center. The control representing spontaneous migration towards lower chamber containing 1% FBS and the images acquired in the *top* and *bottom* of the wells are provided in Figs. S7–S9. Images were acquired with Microscope Leica DMi8, 10× magnification. FBS, fetal bovine serum; UHMK1, U2AF Homology MotifKinase 1.

splicing and it applies to many target genes. A reporter assay confirmed that UHMK1 influences splicing *in vivo* and showed that this effect is dependent on the UHMK1 kinase activity. These data, together with the knowledge that UHMK1 regulates the phosphorylation of a complex network of splicing factors, suggest that UHMK1 function on splicing is more indirect, through the action of the various splicing related factors as well as kinases (AHNAK, PRPF4B) and phosphatases (PPP4R2) regulated by UHMK1.

We showed that the expression of ectopic UHMK1^{WT} was able to increase the SF1-mediated splicing of a reporter gene. SF1 is a well-known substrate of UHMK1 *in vitro* (4, 5, 10, 38). We identified SF1 as the most significant DPP in our phosphoproteome analysis, confirming that UHMK1 controls the phosphorylation status of the SF1 S80 S82 residues (SPSP motif) *in vivo*. However, our observation that only S82 was significantly upregulated in UHMK1-KD and downregulated in UHMK1^{WT} overexpression, while both S80 and S82 were significantly downregulated in UHMK1^{K54R} is quite puzzling and suggests that a complex and rather indirect regulation of SF1 by UHMK1 *in vivo* is likely. Supporting this idea, the expression of UHMK1 was unable to increase the incorporation of radioactive phosphate on full-length SF1 in mammalian cells (4). Moreover, the SF1 SPSP motif is normally found in a highly phosphorylated state in proliferating cells (38), and a subset of SF1 remains phosphorylated in UHMK1 KO mice (11). Besides UHMK1, SRPK2 is also known to phosphorylate the SF1 SPSP motif, preferentially at the residue S82 (39). Thus, the SF1 SPSP motif is likely to be regulated by different kinases and phosphatases (10). Interestingly, the Serine/threonine-protein phosphatase 4 regulatory subunit 2 (*Ppp4r2*) was found upregulated in UHMK1^{WT}-expressing cells and the Serine/threonine-protein kinase PRP4 homolog (*Prpf4b*) was found upregulated in UHMK1-KD cells, making it tempting to speculate that these enzymes could be responsible for the SF1 SPSP dephosphorylation and phosphorylation observed in these respective conditions. Yet, we cannot rule out that the reversed phosphorylation pattern observed on SF1 SPSP motif was due to the cell context or, most likely, to prolonged exposure to UHMK1 modulation in our experimental conditions. The stable UHMK1 knockdown and overexpression approach gives the cells time to accommodate and compensate for the loss or the prolonged activity of the kinase. It is reasonable to think that the interconnection and redundancy of the regulatory signaling network would likely be responsible for compensation, leading to the regulation of indirect targets, which would explain the opposite direction in phosphorylation observed among some of the UHMK1-regulated phosphosites. This idea is in line with previous studies addressing the consequences of long-term perturbation of kinases (40, 41). Altogether, we showed that UHMK1 is the kinase controlling the phosphorylation status of SF1 SPSP motif *in vivo* and that the regulatory mechanism is complex and might involve additional players other than a direct UHMK1-targeted substrate regulation as previously described (4).

It is well accepted that mRNA splicing and transcription are coupled events, and as such, one affects the other (42). Similarly, capping, cleavage, and polyadenylation occur cotranscriptionally. Moreover, the chromatin state and the type of promoter influence the recruitment of transcription and splicing factors, as well as the kinetics of RNA pol II, which in turn influences mRNA transcription rate and alternative splicing (43). Indeed, the RNA-related proteins found in our phosphoproteome data are involved in several steps controlling gene expression, from chromatin modification to mRNA splicing and cleavage to generate mature rRNA (Fig. 9).

Splicing-associated chromatin signatures, characterized by the combination of specific histone marks, have been recently described as a mechanism to rapidly adjust alternative splicing (44). Here, we found that the phosphorylation on S743 of SETD2, a histone lysine methyltransferase responsible for H3 lysine 36 trimethylation (H3K36me3), is upregulated in UHMK1^{WT}. Moreover, a predicted protective ASE transcript of *Setd2* was identified in UHMK1-KD (not shown). Besides SETD2, other chromatin modifier enzymes (SUV39H2, L3MBTL2, NCOR2, ARID1A, CUL4B) were found differentially phosphorylated in our study.

Finally, the UHMK1-mediated regulation of proteins involved in rRNA processing, namely pre-rRNA 2′-O-ribose RNA methyltransferase FTSJ3 (*Ftsj3*), Ribosome biogenesis protein BOP1 (*Bop1*), Nucleophosmin (*Npm1*), and U3 small nucleolar ribonucleoprotein protein MPP10 (*Mphosph10*) is a new finding. This points to a specific role of UHMK1 in the control of rRNA processing and ribosome biogenesis. These processes are closely associated with protein translation (45). In fact, UHMK1 regulated the phosphorylation of eight translation factors: EF-2 (*Eef2*), Translation initiation factor eIF-2B subunit epsilon (*Eif2b5*), eIF-2-beta (*Eif2s2*), EF-1-delta (*Eef1d*), EF-1-gamma (*Eef1g*), eIF4E-binding protein 1 (*Eif4ebp1*), eIF-4-gamma 1 (*Eif4g1*), and ATP-binding cassette sub-family F member 1 (*Abcf1*). Taken together, our results show that UHMK1 controls phosphorylation of proteins involved in different steps of gene expression regulation. This is in agreement with our previous report where we showed that UHMK1 could influence the expression of a report gene (34) and with other studies showing the effect of UHMK1 on gene expression (11, 14, 22).

Intriguingly, in our RNA-seq analysis, UHMK1 knockdown had a limited impact on transcript expression levels, with the identification of 32 differentially expressed genes (DEGs). Nevertheless, some of the gene signatures retrieved from the GSEA analysis relate to the biological processes identified in the GO analysis of phosphoproteome data (Protein complex assembly/disassembly, Microtubule and cytoskeleton organization, Amine/nitrogen metabolic processes, RNA modification, Cell-cycle and Cell division), indicating the involvement of UHMK1 in these processes at both posttranslational and gene expression levels. Moreover, the GSEA analysis pointed to EMT as one of the enriched gene sets. Among the DEGs found in this study, *Prrx1* (46, 47), *Pimreg* (48), *Sptbn1* (49, 50), *Lox* (51), *Memo1* (52), and *Map3k3* (53, 54) were previously

ASBMB

implicated in EMT. Therefore, our study provides new evidence for the association of UHMK1 function with EMT.

In a previous report, we showed that the protein coded by *Pimreg* interacts with UHMK1 and is phosphorylated by this kinase *in vitro* and suggested that the PIMREG–UHMK1 interaction could be important in controlling cell proliferation and gene expression (34). Recently, we showed that PIMREG is involved in DNA damage response (55). Interestingly, our phosphoproteome analysis showed that UHMK1 does not only phosphorylate PIMREG but also other proteins related to DNA damage response, namely RAD54-like, THRAP3, BCLAF1, and TPT1 (56–60), besides PIMREG. Phosphorylation on S128 of PIMREG was significantly upregulated in UHMK1 knockdown and downregulated in UHMK1^{WT} and UHMK1^{K54R} overexpression (although these phosphosites did not cross our fold change cutoff). The residue S128 in mouse corresponds to S131 in human, the reported phosphorylation site of UHMK1 (34). Interestingly, as described here for SF1, phosphorylation of PIMREG by UHMK1 *in vivo* exhibited a reverse phosphorylation pattern from what has been observed *in vitro* when using part of the protein or synthetic peptides as substrates. The fact that *Pimreg* was identified among the DEGs points to a complex regulatory network between these proteins *in vivo*, triggering questions for further investigation.

UHMK1 regulated phosphosites of 30 proteins involved in cell cycle regulation. One third of the cell cycle–related proteins were also annotated as cytoskeleton-related, and the majority of them is also annotated in the BP terms "microtubule cytoskeleton organization", "cell division", and "mitotic cell division". To validate this finding, we performed *in vitro* functional assays to evaluate the phenotypes related to these cellular processes in UHMK1-overexpressing and UHMK1-depleted cells.

Our functional experiments demonstrated that UHMK1^{WT} overexpression decreased the number of colonies formed, while UHMK1 knockdown decreased proliferation. Furthermore, UHMK1 knockdown reduced migration, while UHMK1 overexpression increased migration. These results are in line with previous reports, showing that modulation of UHMK1 affects cell migration, colony formation, and proliferation (13, 16, 25) and further support the data that UHMK1 regulates the phosphorylation of protein networks governing these cellular processes.

Conclusion

A combination of phosphoproteome and transcriptome analysis allowed us to improve the understanding of the role of UHMK1 in cellular processes that have been previously associated with this kinase, particularly in RNA metabolism and splicing. We demonstrated for the first time the effect of UHMK1 modulation on ASEs and on the phosphorylation of a variety of splicing factors, implicating UHMK1 as a novel splicing regulatory kinase. Our data further supports a function of UHMK1 in the modulation of transcription and gene expression, through the regulation of proteins that act in different layers controlling gene expression including chromatin modification, RNA pol II regulation, spliceosome machinery, and mRNA stability, besides rRNA cleavage and protein translation. The general picture of our study is that UHMK1 controls phosphorylation of proteins, gene expression, and alternative splicing of targets that are involved in key cellular processes such as cell cycle, cell division, and microtubule organization.

Experimental procedures

Cell lines and culture conditions

The murine NIH3T3 and the human HEK 293T cell lines were obtained from the *Deutsche Sammlung von Mikroorganismen und Zellkulturen* (DSMZ). Cells were cultured in Dulbecco's modified Eagle's medium supplemented with 10% of fetal bovine serum (FBS) and 1% of the antibiotic penicillin/streptomycin (PAN Biotech), at 37 °C and 5% CO_2. The cell lines were tested for *mycoplasma* using MycoAlert PLUS *Mycoplasma* Detection Kit (Lonza).

Plasmid construction

The WT rat *Uhmk1* coding sequence (UHMK1^{WT}), in frame with an N-terminal Flag peptide, was cloned into the pMSCV-IRES-YFP (MIY) retroviral vector. The UHMK1 kinase-dead mutant (UHMK1^{K54R}) was generated by introducing the K54R mutation in the MIY-Flag-Uhmk1 construct, using the QuickChange II XL Site Directed Mutagenesis kit (Agilent Technologies) and the following primers: forward 5′-CCCCGG CGCCCTCAGGCAGTTCCTG-3′, reverse 5′-CAGGAACT GCCTGAGGGCGCCGGGG-3′. For UHMK1 knockdown (UHMK1-KD), shRNA sequences targeting the murine *Uhmk1* gene were designed using the BLOCK-IT RNAi Designer tool (Invitrogen), cloned into the MSCV-U3-H1-Stuffer entry vector digested with BglII and HindIII, and subcloned into the retroviral vector pMSCV-puromycin-IRES-EGFP siRNA digested with the NotI and ScaI (61). Target sequences are as follows: shUHMK1#1: 5′-GCAAACAGTTCTGCTATTA-3′, shUHMK 1#2: 5′-GCTGGATGATGATTACCTTGA-3′, shUHMK1#3: 5′-GCACTGGATGCTCTAATAA-3′. The scrambled control sequence is (shCTRL): 5′-GCATAGGCTCGAATTCTAA-3′. To express GFP-tagged human SF1, a GFP fragment was amplified from pEGFP-C1 and inserted by restriction-free cloning (62) in plasmid pCDNA3-SF1 (38) to get the plasmid pCDNA3-SF1-GFP-myc. For the expression of GFP-SUGP1, the complementary DNA (cDNA) of human SUGP1 in pENTR223 (DNASU HsCD00516189) was transferred to pDEST-3xFlag-GFP (addgene #122845) by Gateway LR cloning (63). For the expression of GST-SUGP1 in bacteria, a DNA fragment corresponding to residues 326 to 477 of human SUGP1 was amplified and cloned in pGEX6P1 using BamHI and EcoRI sites. Plasmids for expression of recombinant SF1 (residues 1–255) (4) and rat UHMK1 have been described previously (5, 64).

Generation of stable lines by retrovirus production and transduction of NIH3T3 cells

To produce retroviral particles carrying UHMK1^{WT}, UHMK1^{K54R}, or shRNA-UHMK1 sequences, HEK 293T cells

were cotransfected with the retroviral construct and the packaging plasmid pCL-Eco (65), using PEI. The virus-containing media, supplemented with protamine sulfate (5 μg/ml) was used for NIH3T3 cell infection. Transduced cells were sorted by Fluorescence-Activated Cell Sorting (FACS) based on YFP (UHMK1 overexpression) and GFP (UHMK1 knockdown) expression.

Immunoblotting

Cells were lysed in lysis buffer [50 mM Tris pH 8.5, 150 mM NaCl and 1% Triton X-100 and protease inhibitor cocktail (Halt Protease Inhibitor Single-Use Cocktail; Thermo Fisher Scientific)]. Total protein extracts were separated by electrophoresis on 10% SDS-polyacrylamide gel and transferred to a TransBlot Turbo Mini Size polyvinylidene difluoride membrane using the TransBlot Turbo system (BioRad Laboratories, Inc). The membranes were blocked with low-fat milk and probed with primary antibody, followed by secondary antibodies conjugated to horseradish peroxidase. The proteins were detected by chemiluminescence with Pierce ECL Plus Western Blot Substrate (Thermo Fisher Scientific Scientific) and images were captured with Fusion SL (Vilber Loumart). Primary antibodies were anti-UHMK1 (KIS-3B12, 1:10) (11), anti-GFP (sc-8334, 1:4000), and anti-Actin (sc-1616, 1:1000). Secondary antibodies were anti-rat (sc-2006, 1:2000) and anti-rabbit (sc-2313, 1:2000 or 1:8000). Except for anti-UHMK1, all antibodies were purchased from Santa Cruz Biotechnology.

Cell lysis, protein digestion, TMT labeling, and phosphopeptide enrichment

UHMK1-overexpressing and UHMK1-depleted NIH3T3 cells were seeded in 100 mm plates at a density of 1.5×10^6 cells/plate. After 24 h, cells were harvested and lysed in lysis buffer [8 M urea, 80 mM Tris–HCL pH 7.6 and 1X Halt EDTA-free Protease Inhibitor Single-Use Cocktail (Thermo Fisher Scientific) and 1X Phosphatase Inhibitor Cocktail 1, 2, and 3, (Sigma-Aldrich)] at constant rotation, for 45 min at 4 °C. Whole-cell extracts were cleared by centrifugation (16,000*g*, 30 min, and 4 °C), and protein concentrations were determined by the BCA assay. After reduction of disulfide bonds using 10 mM DTT (30 °C, 30 min) and alkylation of cysteine residues using 50 mM chloroacetamide (room temperature, 30 min, in the dark), lysates were diluted to 1.6 M urea using 40 mM Tris–HCl (pH 7.6). Digestion was performed by adding Lys-C and trypsin (1:100 (wt/wt) and 1:50 (wt/wt) enzyme-to-protein ratio, respectively) and incubating at 29 °C overnight. Samples were acidified to a final concentration of 0.5% formic acid to stop the digestion. Digested peptides were desalted using 50 mg, tC18 SepPak cartridges (Waters Corp). The peptide concentration was estimated by NanoDrop measurements, and 70 μg of peptides from each sample were subsequently dried down in a SpeedVac, resuspended in 50 mM Hepes (pH 8.5) and labeled with TMT reagent (Thermo Fisher Scientific, Lot TF270347, Channel 126C, 127N, 128C, 129N, 130C, 131N were used) as described previously (66). Next, all channels were pooled, vacuum dried, and desalted by SepPak cartridges. Peptide solutions were dried down in a SpeedVac and subjected to phosphopeptide enrichment using Fe-IMAC as previously described (67). Flow-through was collected and dried down for further full proteome LC-MS/MS measurements. Phosphopeptides were eluted, dried down, and subjected to fractionation using self-packed StageTips (6 disks, Ø 1.5 mm, C18 material, 3M Empore), as previously described (68). Six fractions of phosphoproteome samples were dried down until further LC-MS/MS measurements.

LC-MS/MS measurements

Nanoflow LC-MS/MS measurements were performed by coupling an UltiMate 3000 RSLCnano chromatography system to an Orbitrap Fusion Lumos Tribrid mass spectrometer (Thermo Fisher Scientific). Samples were loaded on an analytical column (75 μm × 45 cm, packed in-house with 3 μm C18 resin; Reprosil Gold, Dr Maisch). Full proteome and phosphoproteome samples were separated using a 60-min linear gradient from 8% to 34% LC solvent B (0.1% formic acid, 5% DMSO in ACN) and a 90-min linear gradient from 4% to 32% LC solvent B, respectively, at a flow rate of 300 nl/min. The mass spectrometer was operated in data-dependent acquisition mode and positive ionization mode. Full-scan MS1 spectra (m/z 360–1500) were recorded in the Orbitrap at a resolution of 60,000 and with an automatic gain control (AGC) target value of 4e5 and maximum injection time (maxIT) of 50 ms. For peptide identification in full proteome, peptides were fragmented by collision-induced dissociation at 35% normalized collision energy (NCE) and the resulting MS2 spectra were recorded in the ion trap in rapid mode with an AGC target value of 2e4 and maxIT 60 ms. A cycle time and dynamic exclusion were set to 2 and 60 s. For peptide identification in phosphoproteome, peptides were fragmented by collision-induced dissociation at 35% NCE with multistage activation in the ion trap and using an AGC target value of 5e4 and a maxIT of 60 ms. Fragment ions were recorded in Orbitrap at a resolution of 30,000. A cycle time and dynamic exclusion were set to 3 and 90 s. Subsequently, MS3 spectrum for TMT quantification for both full proteome and phosphoproteome were obtained. The peptides were fragmented in the ion trap (AGC of 1.2e5 and maxIT of 120 ms), followed by the synchronous precursor selection of the ten most intense peptide fragments in the ion trap and further fragmentation *via* HCD using an NCE of 55%. The resulting MS3 spectrum was recorded in the Orbitrap at a resolution of 50,000.

Proteomic data analysis

Peptide identification and quantification were performed using MaxQuant v1.6.2.10 (https://www.maxquant.org) (69) with its built-in search engine Andromeda. MS/MS spectra were searched against the UniProt mouse database (55,029 entries, downloaded on 15.07.2019) supplemented with common contaminants. Carbamidomethylated cysteine was set as fixed modification. Oxidation (Met) and N-terminal protein acetylation were set as variable modifications with

phosphorylation (STY) as an additional variable modification for phosphoproteome data. Used channels of TMT10 were specified as label within a reporter ion MS3 experiment type. Isotope impurities of the TMT batch were specified to allow MaxQuant the automated correction of TMT reporter intensities. LysC and Trypsin/P were set as the proteolytic enzymes with up to two missed cleavage sites. Precursor tolerance was set to ±4.5 ppm, and fragment ion tolerance to ±20 ppm. Results were filtered to 1% FDR at peptide spectrum match and protein levels. The MaxQuant results were further analyzed on Microsoft Excel and Perseus platform (v1.6.1.1) (https://maxquant.net/perseus/) (70). First, hits of the reverse and contaminant databases were removed. Data normalization was performed under the assumption that the input amount of each sample is equal across TMT channels. The reporter intensities of full proteome data were median-centered to the overall median of the respective dataset, and the correction factors were calculated. The correction factors of corresponding channels were further applied to the phosphoproteome data. Next, a row-wise normalization was introduced to remove the batch effect as described previously (71). The normalized reporter intensities were log2 transformed and the relative abundances of phosphopeptides were determined. Only phosphopeptides found in all three replicates were considered for the analysis. Differentially phosphorylated phosphopeptides were defined by p-value < 0.05 and fold change of $|1|$. The identified phosphosites were searched in the databases PhosphositePlus (https://www.phosphosite.org/homeAction.action) (72) and PHOSIDA (http://141.61.102.18/phosida/index.aspx) (73).

In vitro *kinase assay*

Recombinant GST-UHMK1, GST-SF1 (residues [1–255]), and GST-SUGP1 (residues [326–477]) were produced in *Escherichia coli* BL21 and purified as previously described (5). Recombinant proteins were quantified by measuring the absorbance at 280 nm and Coomassie staining after SDS-PAGE. For the phosphorylation reaction, 20 pmol of GST-SF1 and GST-SUGP1 served as a substrate for ∼0.2 pmol of recombinant UHMK1, together with 1 mM ATP in a reaction buffer containing Tris–Cl 50 mM pH 8.0, 2 mM EDTA, and 10 mM of $MgCl_2$. The reaction occurred at 30 °C and was stopped after 2 h by adding Laemmli buffer. The samples were denatured at 95 °C for 5 min and separated in a 10% polyacrylamide gel. Next, the gel was stained with Pro-Q Diamond (Invitrogen, Thermo Fisher Scientific) following the manufacturer's instructions. Phosphoproteins were detected using Typhoon laser scanner (Amersham, GE Healthcare), with 532 nm laser. The same gel was then stained with Coomassie Blue and imaged using ChemiDoc (BioRad Laboratories, Inc) or laser scanning at 680 nm. The bands were quantified with Image J (74). Normalization of Pro-Q Diamond (phosphoproteins) relative to Coomassie staining (total protein) was done using the integrated density values.

UHMK1 and SUGP1 coimmunoprecipitation

HEK 293T cells in 35 mm diameter wells were transfected using Lipofectamine 2000 (Thermo Fisher Scientific). Twenty four hours posttransfection, cells were rinsed with PBS and resuspended in 400 µl NP buffer (50 mM Tris–Cl pH 7.5, 150 mM NaCl, and 1% Nonidet P40) with protease inhibitor mix (Roche Diagnostic), PMSF (0.1 mg/ml), and RNase A (10 ng/µl). After vortexing for 30 s, cell extracts were clarified by centrifugation at 20,000*g* for 10 min at 4 °C. The soluble extract was then incubated with 1.2 µg of a mouse anti-GFP antibody (Roche Diagnostic, Cat. Nr. 11814460001) for 1 h at 4 °C and next with 30 µl of protein G Sepharose beads (Cytiva). Beads were washed four times with washing buffer (50 mM Tris–Cl pH 7.5, 150 mM NaCl, and 0.1% Nonidet P40) before resuspension in Laemmli buffer for SDS PAGE analysis. UHMK1 was revealed with the rat monoclonal antibody 3B12 (11) (hybridoma supernatant at 1:20 dilution). GFP-fusion proteins were detected with a rabbit anti-GFP antibody (Santa Cruz SC8334, 1:1000). Primary antibodies were then detected with IRDye680 or IRDye800 secondary antibodies (Li-Cor). Western blots were imaged with Typhoon infrared laser (Amersham, GE Healthcare). Alternatively, gels were imaged using Pro-Q Diamond (Thermo Fisher Scientific) and imaged on the laser scanner at 532 nm. Gels were then restained with Coomassie Blue before scanning at 680 nm.

GO and network analyses of the DPPs

GO analysis and Reactome pathway analysis were carried out using the Protein Analysis Through Evolutionary Relationships - PANTHER (http://geneontology.org). Terms with FDR <0.05 were considered statistically significant.

The DPPs and UHMK1 were searched for interactions using the STRING database (https://string-db.org) (75). Interactions determined experimentally, registered in curated databases, extracted from text mining or coexpression data were considered, using a medium confidence (0.400) interaction score. Network was clustered using the MCL clustering algorithm, with an inflation parameter of 3.

Consensus motif search and ULM motif analyses

Analysis of the consensus motif flanking the significantly regulated phosphosites was performed using pLogo (27). We considered the phosphosites that are very likely direct substrates of UHMK1, *i.e.*, all the phosphosites that were upregulated in $UHMK1^{WT}$ overexpression and downregulated in UHMK1-KD. Besides, we considered all phosphosites in $UHMK1^{K54R}$. In total, 96 phospho-serines and 5 phospho-threonines were submitted to pLogo analysis. Search for ULM motif on the 28 RNA-related proteins (annotated in the RNA-related BP terms in the GO analysis) was performed using ScanProsite (76) and alignment in Clustal Omega (77). We considered putative ULM domains, those sequences that, beyond the conserved tryptophan, had at least two other conserved amino acids in the assigned positions (before or after the tryptophan), based on the known ULM motifs previously reported (30).

RNA extraction, cDNA library preparation, and RNA sequencing

An independent transduction of NIH3T3 cells overexpressing or depleted of UHMK1 was prepared for the

RNA-seq experiment. 1×10^4 cells of each sample were lysed in 100 µl of RLT Plus Lysis Buffer (Qiagen) supplemented with 1% 2-mercaptoethanol. Replicates were harvested in 3 and 6 consecutive days, for UHMK1 knockdown and overexpression, respectively. A bulk RNA barcoding and sequencing protocol, named Prime-seq (37), was used for library preparation. Briefly, RNA was cleaned up using solid phase reversible immobilization beads (Sera Mag, GE Healthcare Life Sciences) in a homemade bead-binding buffer containing 22% PEG. cDNA was generated by Reverse Transcription mix containing the Maxima H Minus reverse transcriptase (Thermo Fisher Scientific), oligo-dT primer E3V6NEXT, and template switch primer E5V6NEXT. cDNA from all the samples was pooled together pre-amplified using KAPA HiFi HotStart polymerase (Roche) and SingV6 primer. Nextera libraries (5 replicates) were constructed from 0.8 ng of pre-amplified cleaned up cDNA using Nextera XT Kit (Illumina). Index PCR was carried out using the custom P5 primer (P5NEXTPT5) and the i701 Nextera primer (IDT Technologies). Libraries were size selected in a 2% E-Gel Agarose EX Gels (Life Technologies), cut out in the range of 300 to 800 bp, and extracted using the MinElute Kit (Qiagen), according to manufacturer's recommendations.

Single-end sequencing was performed in the Illumina HiSeq 1500 system (Illumina) with a coverage of 74 bp. Raw FASTQ data were processed with the pipeline zUMIs, version 0.2.0 (78) and mapped to the mouse genome mm10 using the software STAR (79). Gene annotations were obtained from Ensembl (GRCm38.75).

RNA-seq data analyses and target validation by qPCR

Differential expression between UHMK1-KD (shUHMK1#1, shUHMK1#2, and shUHMK1#3 data, combined and used as one pseudosample) and shCTRL was assessed using the edgeR/limma package (80, 81). Gene set enrichment analysis was performed using GSEA version 6.2 (82), with gene sets for *Mus musculus* obtained from GO2MSIG (83). Results were regarded as significant with a *p*-value <0.05.

RNA-seq validation was carried out in an independent transduction of NIH3T3 cells, by analyzing the expression of eight DEGs by PCR array (qPCR). The DEGs chosen for validation were as follows: *Cdca4, Fam198b, Pimreg, Lox, Map3k3, Oaz1, Prrx1*, and *Sptbn1*. The cells were cultivated in the same conditions described for RNA-seq. Total RNA was extracted using RNeasy Mini Kit (Qiagen). cDNA was produced using the iScript cDNA Synthesis Kit (Bio-Rad Laboratories). qPCR was performed using PrimePCR custom plates (Bio-Rad Laboratories), containing the lyophilized primers for the selected gene. The housekeeping genes *Gapdh* and *Hprt* were used as endogenous control and relative expression was calculated using the $2^{-\Delta\Delta Cq}$ method (84).

Analysis of alternative splicing

For ASEs detection in the mouse genome (mm10), we considered all raw sequencing reads from the replicates of each condition as four pseudosamples (UHMK1-KD, shCTRL, $UHMK1^{WT}$, and EV) and identified ASEs using Bayesian inference followed by differential analysis from vast-tools pipeline (vast-tools diff module) (85, 86) with $|dPSI| \geq 0.2$ and $MV|dPSI\_at\_95| \geq 0.05$ as significance thresholds. Additional nondefault parameters for vast-tools diff module include the following: -S 1, -e 10, -m 0.05. ASEs were further categorized into functional classifications according to their predicted impact on the ORF: "neutral" for events that generate known functional isoforms or which do not alter the protein sequence (ex. an alternative exon); "protective" for events that reduce the occurrence of deleterious nucleotide sequences and therefore generate a functional protein (ex. removal of an intron/exon containing a premature stop codon), and "disruptive" which denote events that increase the frequency of disruptive sequences in the ORF (ex. inclusion of introns/exons containing premature stop codons or removal of essential exons for protein function) (87). All postprocessing data analysis and figure generation were conducted using custom python3.7 scripts, which are available upon request.

Splicing reporter assays

HEK 293T cells were seeded in 24-well plates at a density of 9×10^4 cells/well. After 24 h, the cells were cotransfected with 200 ng of the pTN24 reporter plasmid (88), MIY-$UHMK1^{WT}$ and MIY-$UHMK1^{K54R}$ (200 ng) construct alone or in combination with pcDNA-SF1(4) (300 ng of each construct). DNA was kept constant at 800 ng DNA in each well and 2 µl of Lipofectamine 2000 (Thermo Fisher Scientific) was used as a transfection reagent. The cells were harvested 24 h later and assayed for luciferase and β-Galactosidase activity using Dual Light Luciferase and β-Galactosidase Reporter Gene Assay System (Thermo Fisher Scientific). The measurements were performed in duplicates in an Infinite F200 Pro microplate reader (Tecan Group Ltd). Splicing was evaluated as a ratio of luciferase/β-galactosidase. Parallel transfections were performed in the same conditions to assess gene expression of $UHMK1^{WT}$, $UHMK1^{K54R}$, and SF1 by qPCR.

Colony forming assay

Cells were seeded in 6-well plates at a density of 750 cells/well. After 6 days of incubation under normal culturing conditions, the colonies were fixed with 70% ethanol for 10 min, stained with 0.05% crystal violet for 10 min, and washed with water. The colonies were counted using an inverted microscope (Motic). A colony was defined by a minimum of 50 cells.

Proliferation assay

Proliferation was evaluated by BrdU incorporation. 2×10^5 cells were seeded in 6-well plates. After 24 h, 10 µM of BrdU was added and incubated for 2 h. BrdU staining was carried out with the APC BrdU Flow Kit (BD Biosciences). Flow cytometry analyses were performed using an FACS Canto (BD Biosciences).

Cell viability assay

Cells were seeded in 96-well plates at a density of 8 × 10^3 cells/well. After 24 h, 20 μl of Cell Titer Blue reagent (Promega,) was added to the cells and incubated for 4 h at 37 °C, protected from light. Fluorescence was measured using Promega GloMax Microplate Reader, excitation filter: 520 nm, emission: 580 to 640.

Apoptosis assay

Cells were seeded in 12-well plates at a density of 1 × 10^5 cells/well. After 24 h, cells were washed with ice-cold DPBS plus 5 mM EDTA and stained with annexin V and PI (BD Biosciences) for 15 min at RT. Analysis was carried out using FACS Canto (BD Biosciences).

Migration assay

Cell cultures were depleted from serum (1% FBS-containing medium without antibiotics) for 16 to 20 h. After that period, 1 × 10^5 cells were seeded directly over an 8 μm membrane in a 96-well Boyden chamber plate. The lower compartment of the chamber was filled with 10% FBS-containing medium. After 24 h, the cells that migrated through the membrane were fixed with 70% ethanol and stained with 0.05% crystal violet, as previously described (89). Images were acquired using Microscope Leica DMi8 at 10× magnification.

Statistical analyses

Statistical analyses (of splicing reporter assays, RNA-seq validation, and functional assays) were carried out on GraphPad Prism version 7.0 for MacOS X (GraphPad Software, available at https://www.graphpad.com). The function Column Statistics was used to evaluate parameters such as median, mean, coefficient of variation, kurtosis, skewness, and normality (Shapiro-Wilk test). Based on these parameters, the tests chosen to evaluate three groups or more were One-way ANOVA followed by Bonferroni's multiple comparison test or Kruskal-Wallis test followed by Dunn's multiple comparison test. For two groups, unpaired Student *t* test or Mann-Whitney test were used. A confidence interval of 0.95 was set and therefore *p*-values lower than 0.05 were regarded as statistically significant.

Data availability

The RNA-seq data from UHMK1-overexpressing or UHMK1-depleted NIH3T3 cells are available in the Gene Expression Omnibus (GEO) repository, accession number GSE199768. The UHMK1 mass spectrometry proteomics data have been deposited to the ProteomeXchange Consortium *via* the Proteomics Identification Database (PRIDE) partner repository with the dataset identifier PXD033353.

Supporting information—This article contains supporting information.

Acknowledgments—We thank Dr Ian C. Eperon for the pTN24 reporter plasmid, Dr Saghi Ghaffari for the MSCV-U3-H1-Stuffer and pMSCV-puromycin IRES2-EGFP siRNA vectors, and Dr Alexander Faussner for the support in the splicing reporter assay readouts.

Author contributions—V. C. A., Y.-C. C., J. W. B., L. M. S. P., S. P., J. M. S., and A. M. investigation; V. C. A., Y.-C. C., J. W. B., P. K., F. E. C., and K. B. M. formal analysis; V. C. A., P. K., and F. E. C. visualization; V. C. A. validation; V. C. A. and L. F. A. writing–original draft; A. M., K. B. M., W. E., B. K., P. A. G., and L. F. A. supervision; A. M., P. A. G., and L. F. A. writing–review and editing; W. E., B. K., and P. A. G. resources; P. A. G. and L. F. A. conceptualization; L. F. A. project administration; L. F. A. funding acquisition.

Funding and additional information—This research was supported by the Coordenação de Aperfeiçoamento Pessoal de Nível Superior (CAPES/PDSE, grant to V. C. A. and to F. E. C.), Deutsche Forschungsgemeinschaft (DFG-SFB1309, grant to Y.-C. C.), and the Fundação de Amparo à Pesquisa do Estado de São Paulo (FAPESP 2020/02006-0 to K. B. M., 2014/01458-3 and 2022/08648-9 to L. F. A.). P. A. G. acknowledges support by the Wilhelm Sander-Stiftung (Förderantrag Nr. 2014.162.3) and the Munich Clinician Scientist Program (MCSP).

Conflict of interest—The authors declare that they have no conflicts of interest with the contents of this article.

Abbreviations—The abbreviations used are: AGC, automatic gain control; ASE, alternative splicing event; BP, Biological processs; DEG, differentially expressed gene; DPP, differentially phosphorylated protein; EMT, Epithelial Mesenchymal Transition; EV, empty vector; FACS, Fluorescence-Activated Cell Sorting; FBS, fetal bovine serum; FDR, false discovery rate; GO, gene ontology; GSEA, Gene Set Enrichment Analysis; maxIT, maximum injection time; NCE, normalized collision energy; PSI, percent spliced in; qPCR, quantitative PCR; UHM, U2AF homology motif; UHMK1, U2AF Homology Motif Kinase 1; ULM, UHM ligand motif.

References

1. Ardito, F., Giuliani, M., Perrone, D., Troiano, G., and Lo Muzio, L. (2017) The crucial role of protein phosphorylation in cell signaling and its use as targeted therapy. *Int. J. Mol. Med.* **40**, 271–280
2. Maucuer, A., Le Caer, J. P., Manceau, V., and Sobel, A. (2000) Specific Ser-Pro phosphorylation by the RNA-recognition motif containing kinase KIS. *Eur. J. Biochem.* **267**, 4456–4464
3. Kielkopf, C. L., Lücke, S., and Green, M. R. (2004) U2AF homology motifs: protein recognition in the RRM world. *Genes Dev.* **18**, 1513–1526
4. Manceau, V., Swenson, M., Le Caer, J. P., Sobel, A., Kielkopf, C. L., and Maucuer, A. (2006) Major phosphorylation of SF1 on adjacent Ser-Pro motifs enhances interaction with U2AF65. *FEBS J.* **273**, 577–587
5. Manceau, V., Kielkopf, C. L., Sobel, A., and Maucuer, A. (2008) Different requirements of the kinase and UHM domains of KIS for its nuclear localization and binding to splicing factors. *J. Mol. Biol.* **381**, 748–762
6. Berglund, J. A., Chua, K., Abovich, N., Reed, R., and Rosbash, M. (1997) The splicing factor BBP interacts specifically with the pre-mRNA branchpoint sequence UACUAAC. *Cell* **89**, 781–787
7. Corioni, M., Antih, N., Tanackovic, G., Zavolan, M., and Krämer, A. (2011) Analysis of *in situ* pre-mRNA targets of human splicing factor SF1 reveals a function in alternative splicing. *Nucleic Acids Res.* **39**, 1868–1879
8. Tanackovic, G., and Krämer, A. (2005) Human splicing factor SF3a, but not SF1, is essential for pre-mRNA Splicing *in vivo*. *Mol. Biol. Cell.* **16**, 1366–1377
9. Hahn, C. N., Venugopal, P., Scott, H. S., and Hiwase, D. K. (2015) Splice factor mutations and alternative splicing as drivers of hematopoietic malignancy. *Immunol. Rev.* **263**, 257–278

10. Chatrikhi, R., Wang, W., Gupta, A., Loerch, S., Maucuer, A., and Kielkopf, C. L. (2016) SF1 phosphorylation enhances specific binding to U2AF65 and reduces binding to 3′-splice-site RNA. *Biophys. J.* **111**, 2570–2586
11. Manceau, V., Kremmer, E., Nabel, E. G., and Maucuer, A. (2012) The protein kinase KIS impacts gene expression during development and fear conditioning in adult mice. *PLoS One* **7**, 1–11
12. Boehm, M., Yoshimoto, T., Crook, M. F., Nallamshetty, S., True, A., Nabel, G. J., *et al.* (2002) A growth factor-dependent nuclear kinase phosphorylates p27(Kip1) and regulates cell cycle progression. *EMBO J.* **21**, 3390–3401
13. Langenickel, T. H., Olive, M., Boehm, M., San, H., Crook, M. F., and Nabel, E. G. (2008) KIS protects against adverse vascular remodeling by opposing stathmin-mediated VSMC migration in mice. *J. Clin. Invest.* **118**, 3848–3859
14. Francone, V. P., Ifrim, M. F., Rajagopal, C., Leddy, C. J., Wang, Y., Carson, J. H., *et al.* (2010) Signaling from the secretory granule to the nucleus. *Mol. Endocrinol.* **24**, 1543–1558
15. Cambray, S., Pedraza, N., Rafel, M., Gari, E., Aldea, M., and Gallego, C. (2009) Protein kinase KIS localizes to RNA granules and enhances local translation. *Mol. Cell. Biol.* **29**, 726–735
16. Barbutti, I., Machado-Neto, J. A., Arfelli, V. C., de Melo Campos, P., Traina, F., Saad, S. T. O., *et al.* (2018) The U2AF homology motif kinase 1 (UHMK1) is upregulated upon hematopoietic cell differentiation. *Biochim. Biophys. Acta Mol. Basis Dis.* **1864**, 959–966
17. Choi, H. J., Park, H., Zhang, L., Kim, J. H., Kim, Y. A., Yang, J. Y., *et al.* (2016) Genome-wide association study in East Asians suggests UHMK1 as a novel bone mineral density susceptibility gene. *Bone* **91**, 113–121
18. Alam, M. R., Caldwell, B. D., Johnson, R. G., Darlington, D. N., Mains, R. E., and Eipper, B. A. (1996) Novel proteins that interact with the COOH-terminal cytosolic routing determinants of an integral membrane peptide-processing enzyme. *J. Biol. Chem.* **271**, 28636–28640
19. Caldwell, B. D., Darlington, D. N., Penzes, P., Johnson, R. C., Eipper, B. A., and Mains, R. E. (1999) The novel kinase peptidylglycine alpha-amidating monooxygenase cytosolic interactor protein 2 interacts with the cytosolic routing determinants of the peptide processing enzyme peptidylglycine alpha-amidating monooxygenase. *J. Biol. Chem.* **274**, 34646–34656
20. Alam, M. R., Steveson, T. C., Johnson, R. C., Bäck, N., Abraham, B., Mains, R. E., *et al.* (2001) Signaling mediated by the cytosolic domain of peptidylglycine alpha-amidating monooxygenase. *Mol. Biol. Cell.* **12**, 629–644
21. Pedraza, N., Ortiz, R., Cornado, A., Llobet, A., Aldea, M., and Gallego, C. (2014) KIS, a kinase associated with microtubule regulators, enhances translation of AMPA receptors and stimulates dendritic spine remodeling. *J. Neurosci.* **34**, 13988–13997
22. Wei, T., Weiler, S. M. E., Tóth, M., Sticht, C., Lutz, T., Thomann, S., *et al.* (2019) YAP-dependent induction of UHMK1 supports nuclear enrichment of the oncogene MYBL2 and proliferation in liver cancer cells. *Oncogene* **38**, 5541–5550
23. Chu, Y. De, Lin, W. R., Lin, Y. H., Kuo, W. H., Tseng, C. J., Lim, S. N., *et al.* (2020) COX5B-mediated bioenergetic alteration regulates tumor growth and migration by modulating AMPK-UHMK1-ERK cascade in hepatoma. *Cancers (Basel)* **12**, 1–23
24. Feng, X., Ma, D., Zhao, J., Song, Y., Zhu, Y., Zhou, Q., *et al.* (2020) UHMK1 promotes gastric cancer progression through reprogramming nucleotide metabolism. *EMBO J.* **39**, 1–19
25. Luo, Y., Han, S., Yan, B., Ji, H., Zhao, L., Gladkich, J., *et al.* (2022) UHMK1 is a novel marker for personalized prediction of pancreatic cancer prognosis. *Front. Oncol.* **12**, 1–15
26. Niu, H., Zhao, M., Huang, J., Wang, J., Si, Y., Cheng, S., *et al.* (2022) UHMK1-dependent phosphorylation of cajal body protein coilin alters 5-FU sensitivity in colon cancer cells. *Cell Commun. Signal.* **20**, 1–17
27. O'Shea, J. P., Chou, M. F., Quader, S. A., Ryan, J. K., Church, G. M., and Schwartz, D. (2013) PLogo: a probabilistic approach to visualizing sequence motifs. *Nat. Methods* **10**, 1211–1212
28. Johnson, J. L., Yaron, T. M., Huntsman, E. M., Kerelsky, A., Song, J., Regev, A., *et al.* (2023) An atlas of substrate specificities for the human serine/threonine kinome. *Nature* **613**, 759–766
29. Du, C., Ma, X., Meruvu, S., Hugendubler, L., and Mueller, E. (2014) The adipogenic transcriptional cofactor ZNF638 interacts with splicing regulators and influences alternative splicing. *J. Lipid Res.* **55**, 1886–1896
30. Loerch, S., and Kielkopf, C. L. (2016) Unmasking the U2AF homology motif family: a bona fide protein–protein interaction motif in disguise. *RNA* **22**, 1795–1807
31. Zhang, J., Ali, A. M., Lieu, Y. K., Liu, Z., Gao, J., Rabadan, R., *et al.* (2019) Disease-causing mutations in SF3B1 alter splicing by disrupting interaction with SUGP1. *Mol. Cell.* **76**, 82–95.e7
32. Braunschweig, U., Gueroussov, S., Plocik, A. M., Graveley, B. R., and Blencowe, B. J. (2013) Dynamic integration of splicing within gene regulatory pathways. *Cell* **152**, 1252–1269
33. Maucuer, A., Camonis, J. H., and Sobel, A. (1995) Stathmin interaction with a putative kinase and coiled-coil-forming protein domains. *Proc. Natl. Acad. Sci. U. S. A.* **92**, 3100–3104
34. Archangelo, L. F., Greif, P. A., Maucuer, A., Manceau, V., Koneru, N., Bigarella, C. L., *et al.* (2013) The CATS (FAM64A) protein is a substrate of the Kinase Interacting Stathmin (KIS). *Biochim. Biophys.* **1833**, 1269–1279
35. Stamm, S. (2008) Regulation of alternative splicing by reversible protein phosphorylation. *J. Biol. Chem.* **283**, 1223–1227
36. Naro, C., and Sette, C. (2013) Phosphorylation-mediated regulation of alternative splicing in cancer. *Int. J. Cell Biol.* **2013**, 151839
37. Janjic, A., Wange, L. E., Bagnoli, J. W., Geuder, J., Nguyen, P., Richter, D., *et al.* (2022) Prime-seq, efficient and powerful bulk RNA sequencing. *Genome Biol.* **23**, 1–27
38. Wang, W., Maucuer, A., Gupta, A., Manceau, V., Thickman, K. R., Bauer, W. J., *et al.* (2013) Structure of phosphorylated SF1 bound to U2AF65 in an essential splicing factor complex. *Structure* **21**, 197–208
39. Lipp, J. J., Marvin, M. C., Shokat, K. M., and Guthrie, C. (2015) SR protein kinases promote splicing of nonconsensus introns. *Nat. Struct. Mol. Biol.* **22**, 611–617
40. Bodenmiller, B., Wanka, S., Kraft, C., Urban, J., Campbell, D., Pedrioli, P. G., *et al.* (2010) Phosphoproteomic analysis reveals interconnected system-wide responses to perturbations of kinases and phosphatases in yeast. *Sci. Signal.* **3**, 1–9
41. Klomp, J. E., Shaaya, M., Matsche, J., Rebiai, R., Aaron, J. S., Collins, K. B., *et al.* (2019) Time-variant SRC kinase activation determines endothelial permeability response. *Cell Chem. Biol.* **26**, 1081–1094.e6
42. Tellier, M., Maudlin, I., and Murphy, S. (2020) Transcription and splicing: a two-way street. *Wiley Interdiscip. Rev. RNA* **11**, 1–25
43. Kornblihtt, A. R., Schor, I. E., Alló, M., Dujardin, G., Petrillo, E., and Muñoz, M. J. (2013) Alternative splicing: a pivotal step between eukaryotic transcription and translation. *Nat. Rev. Mol. Cell Biol.* **14**, 153–165
44. Agirre, E., Oldfield, A. J., Bellora, N., Segelle, A., and Luco, R. F. (2021) Splicing-associated chromatin signatures: a combinatorial and position-dependent role for histone marks in splicing definition. *Nat. Commun.* **12**, 1–16
45. Piazzi, M., Bavelloni, A., Gallo, A., Faenza, I., and Blalock, W. L. (2019) Signal transduction in ribosome biogenesis : a recipe to avoid disaster. *Int. J. Mol. Sci.* **20**, 1–47
46. Ocaña, O. H., Córcoles, R., Fabra, Á., Moreno-Bueno, G., Acloque, H., Vega, S., *et al.* (2012) Metastatic colonization requires the repression of the epithelial-mesenchymal transition inducer Prrx1. *Cancer Cell* **22**, 709–724
47. Guo, J., Fu, Z., Wei, J., Lu, W., Feng, J., and Zhang, S. (2015) PRRX1 promotes epithelial–mesenchymal transition through the Wnt/β-catenin pathway in gastric cancer. *Med. Oncol.* **32**, 1–12
48. Zhang, J., Qian, L., Wu, J., Lu, D., Yuan, H., Li, W., *et al.* (2019) Up-regulation of FAM64A promotes epithelial-to-mesenchymal transition and enhances stemness features in breast cancer cells. *Biochem. Biophys. Res. Commun.* **513**, 472–478
49. Zhi, X., Lin, L., Yang, S., Bhuvaneshwar, K., Wang, H., Gusev, Y., *et al.* (2015) βII-Spectrin (SPTBN1) suppresses progression of hepatocellular carcinoma and Wnt signaling by regulation of Wnt inhibitor kallistatin. *Hepatology* **61**, 598–612

50. Chen, S., Li, J., Zhou, P., and Zhi, X. (2020) SPTBN1 and cancer, which links? *J. Cell. Physiol.* **235**, 17–25
51. Kasashima, H., Yashiro, M., Kinoshita, H., Fukuoka, T., Morisaki, T., Masuda, G., *et al.* (2016) Lysyl oxidase is associated with the epithelial–mesenchymal transition of gastric cancer cells in hypoxia. *Gastric Cancer* **19**, 431–442
52. Sorokin, A. V., and Chen, J. (2013) MEMO1, a new IRS1-interacting protein, induces epithelial-mesenchymal transition in mammary epithelial cells. *Oncogene* **32**, 3130–3138
53. Santoro, R., Zanotto, M., Carbone, C., Piro, G., Tortora, G., and Melisi, D. (2018) MEKK3 sustains EMT and stemness in pancreatic cancer by regulating YAP and TAZ transcriptional activity. *Anticancer Res.* **38**, 1937–1946
54. Stevens, M. V., Broka, D. M., Parker, P., Rogowitz, E., Vaillancourt, R. R., and Camenisch, T. D. (2008) MEKK3 initiates TGFβ2-dependent EMT during endocardial cushion morphogenesis. *Circ. Res.* **103**, 1430–1440
55. Serafim, R. B., Cardoso, C., Arfelli, V. C., Valente, V., and Archangelo, L. F. (2022) PIMREG expression level predicts glioblastoma patient survival and affects temozolomide resistance and DNA damage response. *Biochim. Biophys. Acta Mol. Basis Dis.* **1868**, 166382
56. Heyer, W. D., Li, X., Rolfsmeier, M., and Zhang, X. P. (2006) Rad54: the swiss army knife of homologous recombination? *Nucleic Acids Res.* **34**, 4115–4125
57. Wright, W. D., and Heyer, W. D. (2014) Rad54 functions as a heteroduplex DNA pump modulated by its DNA substrates and Rad51 during D loop formation. *Mol. Cell* **53**, 420–432
58. Vohhodina, J., Barros, E. M., Savage, A. L., Liberante, F. G., Manti, L., Bankhead, P., *et al.* (2017) The RNA processing factors THRAP3 and BCLAF1 promote the DNA damage response through selective mRNA splicing and nuclear export. *Nucleic Acids Res.* **45**, 12816–12833
59. Neuhäuser, K., Küper, L., Christiansen, H., and Bogdanova, N. (2019) Assessment of the role of translationally controlled tumor protein 1 (TPT1/TCTP) in breast cancer susceptibility and ATM signaling. *Clin. Transl. Radiat. Oncol.* **15**, 99–107
60. Zhang, J., De Toledo, S. M., Pandey, B. N., Guo, G., Pain, D., Li, H., *et al.* (2012) Role of the translationally controlled tumor protein in DNA damage sensing and repair. *Proc. Natl. Acad. Sci. U. S. A.* **109**, E926–E933
61. Ghaffari, S., Kitidis, C., Zhao, W., Marinkovic, D., Fleming, M. D., Luo, B., *et al.* (2006) AKT induces erythroid-cell maturation of JAK2-deficient fetal liver progenitor cells and is required for Epo regulation of erythroid-cell differentiation. *Blood* **107**, 1888–1891
62. Bond, S. R., and Naus, C. C. (2012) RF-Cloning.org: an online tool for the design of restriction-free cloning projects. *Nucleic Acids Res.* **40**, 209–213
63. Katzen, F. (2007) Gateway® recombinational cloning: a biological operating system. *Expert Opin. Drug Discov.* **2**, 571–589
64. Maucuer, A., Ozon, S., Manceau, V., Gavet, O., Lawler, S., Curmi, P., *et al.* (1997) KIS is a protein kinase with an RNA recognition motif. *J. Biol. Chem.* **272**, 23151–23156
65. Naviaux, R. K., Costanzi, E., Haas, M., and Verma, I. M. (1996) The pCL vector system: rapid production of helper-free, high-titer, recombinant retroviruses. *J. Virol.* **70**, 5701–5705
66. Zecha, J., Satpathy, S., Kanashova, T., Avanessian, S. C., Kane, M. H., Clauser, K. R., *et al.* (2019) TMT labeling for the masses: a robust and cost-efficient, in-solution labeling approach. *Mol. Cell. Proteomics* **18**, 1468–1478
67. Ruprecht, B., Koch, H., Domasinska, P., Frejno, M., Kuster, B., and Lemeer, S. (2017) Optimized enrichment of phosphoproteomes by Fe-IMAC column chromatography. In Comai, L., Katz, J., Mallick, P., eds., *Proteomics: Methods and Protocols* (vol. 1550,. Springer, New York, NY: 47–60
68. Ruprecht, B., Zecha, J., Zolg, D. P., and Kuster, B. (2017) High pH reversed-phase micro-columns for simple, sensitive, and efficient fractionation of proteome and (TMT labeled) phosphoproteome digests. In: Comai, L., Katz, J., Mallick, P., eds. *Proteomics: Methods and Protocols*, Springer, New York, NY: 83–98
69. Tyanova, S., Temu, T., and Cox, J. (2016) The MaxQuant computational platform for mass spectrometry-based shotgun proteomics. *Nat. Protoc.* **11**, 2301–2319
70. Tyanova, S., Temu, T., Sinitcyn, P., Carlson, A., Hein, M. Y., Geiger, T., *et al.* (2016) The Perseus computational platform for comprehensive analysis of (prote)omics data. *Nat. Methods* **13**, 731–740
71. Zecha, J., Meng, C., Zolg, D. P., Samaras, P., Wilhelm, M., and Kuster, B. (2018) Peptide level turnover measurements enable the study of proteoform dynamics. *Mol. Cell. Proteomics* **17**, 974–992
72. Hornbeck, P. V., Zhang, B., Murray, B., Kornhauser, J. M., Latham, V., and Skrzypek, E. (2015) PhosphoSitePlus, 2014: mutations, PTMs and recalibrations. *Nucleic Acids Res.* **43**, 512–520
73. Gnad, F., Ren, S., Cox, J., Olsen, J. V., Macek, B., Oroshi, M., *et al.* (2007) PHOSIDA (phosphorylation site database): management, structural and evolutionary investigation, and prediction of phosphosites. *Genome Biol.* **8**, 1–13
74. Schneider, C. A., Rasband, W. S., and Eliceiri, K. W. (2012) NIH image to ImageJ: 25 years of image analysis. *Nat. Methods* **9**, 671–675
75. Szklarczyk, D., Gable, A. L., Lyon, D., Junge, A., Wyder, S., Huerta-Cepas, J., *et al.* (2019) STRING v11: Protein-protein association networks with increased coverage, supporting functional discovery in genome-wide experimental datasets. *Nucleic Acids Res.* **47**, D607–D613
76. de Castro, E., Sigrist, C. J. A., Gattiker, A., Bulliard, V., Langendijk-Genevaux, P. S., Gasteiger, E., *et al.* (2006) ScanProsite: detection of PROSITE signature matches and ProRule-associated functional and structural residues in proteins. *Nucleic Acids Res.* **34**, 362–365
77. Sievers, F., and Higgins, D. G. (2014) Clustal omega, accurate alignment of very large numbers of sequences. In: Russel, D. J., ed., **1079**. *Multiple Sequence Alignment Methods, Methods in Molecular Biology*, Springer Science+Business Media, Berlin: 105–116
78. Parekh, S., Ziegenhain, C., Vieth, B., Enard, W., and Hellmann, I. (2018) zUMIs - a fast and flexible pipeline to process RNA sequencing data with UMIs. *Gigascience* **7**, 1–9
79. Dobin, A., Davis, C. A., Schlesinger, F., Drenkow, J., Zaleski, C., Jha, S., *et al.* (2013) Star: ultrafast universal RNA-seq aligner. *Bioinformatics* **29**, 15–21
80. Ritchie, M. E., Phipson, B., Wu, D., Hu, Y., Law, C. W., Shi, W., *et al.* (2015) Limma powers differential expression analyses for RNA-sequencing and microarray studies. *Nucleic Acids Res.* **43**, e47
81. Robinson, M. D., McCarthy, D. J., and Smyth, G. K. (2010) edgeR: a bioconductor package for differential expression analysis of digital gene expression data. *Bioinformatics* **26**, 139–140
82. Subramanian, A., Tamayo, P., Mootha, V. K., Mukherjee, S., Ebert, B. L., Gillette, M. A., *et al.* (2005) Gene set enrichment analysis: a knowledge-based approach for interpreting genome-wide expression profiles. *Proc. Natl. Acad. Sci. U. S. A.* **102**, 15545–15550
83. Powell, J. A. C. (2014) GO2MSIG, an automated GO based multi-species gene set generator for gene set enrichment analysis. *BMC Bioinformatics* **15**, 1–6
84. Livak, K. J., and Schmittgen, T. D. (2001) Analysis of relative gene expression data using real-time quantitative PCR and the 2-ΔΔCT method. *Methods* **25**, 402–408
85. Tapial, J., Ha, K. C. H., Sterne-Weiler, T., Gohr, A., Braunschweig, U., Hermoso-Pulido, A., *et al.* (2017) An atlas of alternative splicing profiles and functional associations reveals new regulatory programs and genes that simultaneously express multiple major isoforms. *Genome Res.* **27**, 1759–1768
86. Han, H., Braunschweig, U., Gonatopoulos-Pournatzis, T., Weatheritt, R. J., Hirsch, C. L., Ha, K. C. H., *et al.* (2017) Multilayered control of alternative splicing regulatory networks by transcription factors. *Mol. Cell.* **65**, 539–553
87. Irimia, M., Weatheritt, R. J., Ellis, J. D., Parikshak, N. N., Gonatopoulos-Pournatzis, T., Babor, M., *et al.* (2014) A highly conserved program of neuronal microexons is misregulated in autistic brains. *Cell* **159**, 1511–1523
88. Nasim, M. T., Chowdhury, H. M., and Eperon, I. C. (2002) A double reporter assay for detecting changes in the ratio of spliced and unspliced mRNA in mammalian cells. *Nucleic Acids Res.* **30**, e109

89. Justus, C. R., Leffler, N., Ruiz-Echevarria, M., and Yang, L. V. (2014) *In vitro* cell migration and invasion assays. *J. Vis. Exp.* https://doi.org/10.3791/51046
90. Uniprot. (2019) UniProt: a worldwide hub of protein knowledge. *Nucleic Acids Res.* **47**, 506–515
91. Cvitkovic, I., and Jurica, M. S. (2013) Spliceosome database: a tool for tracking components of the spliceosome. *Nucleic Acids Res.* **41**, 132–141
92. Braun, J. E., Huntzinger, E., Fauser, M., and Izaurralde, E. (2011) GW182 proteins directly recruit cytoplasmic deadenylase complexes to miRNA targets. *Mol. Cell.* **44**, 120–133
93. Sagawa, F., Ibrahim, H., Morrison, A. L., Wilusz, C. J., and Wilusz, J. (2011) Nucleophosmin deposition during mRNA 3′ end processing influences poly(A) tail length. *EMBO J.* **30**, 3994–4005
94. Charenton, C., and Graille, M. (2018) mRNA decapping: finding the right structures. *Philos. Trans. R. Soc. B Biol. Sci.* **373**, 1–11
95. Ivanova, I., Much, C., Di Giacomo, M., Azzi, C., Morgan, M., Moreira, P. N., *et al.* (2017) The RNA m6A reader YTHDF2 is essential for the post-transcriptional regulation of the maternal transcriptome and oocyte competence. *Mol. Cell* **67**, 1059–1067.e4
96. Lee, K. M., Hsu, I. W., and Tarn, W. Y. (2010) TRAP150 activates pre-mRNA splicing and promotes nuclear mRNA degradation. *Nucleic Acids Res.* **38**, 3340–3350
97. Pfeiffer, J. R., McAvoy, B. L., Fecteau, R. E., Deleault, K. M., and Brooks, S. A. (2011) CARHSP1 is required for effective tumor necrosis factor alpha mRNA stabilization and localizes to processing bodies and exosomes. *Mol. Cell. Biol.* **31**, 277–286
98. Liu, H.-W., Banerjee, T., Guan, X., Freitas, M. A., and Parvin, J. D. (2015) The chromatin scaffold protein SAFB1 localizes SUMO-1 to the promoters of ribosomal protein genes to facilitate transcription initiation and splicing. *Nucleic Acids Res.* **43**, 3605–3613
99. Lindström, M. S. (2011) NPM1/B23: a multifunctional chaperone in ribosome biogenesis and chromatin remodeling. *Biochem. Res. Int.* **2011**, 1–16
100. Davies, J. S., Klein, D. C., and Carter, D. A. (2011) Selective genomic targeting by FRA-2/FOSL2 transcription factor: regulation of the Rgs4 gene is mediated by a variant activator protein 1 (AP-1) promoter sequence/creb-binding protein (CBP) mechanism. *J. Biol. Chem.* **286**, 15227–15239
101. Kaitsuka, T., Tomizawa, K., and Matsushita, M. (2011) Transformation of eEF1Bdelta into heat-shock response transcription factor by alternative splicing. *EMBO Rep.* **12**, 673–681
102. De Almeida, S. F., Grosso, A. R., Koch, F., Fenouil, R., Carvalho, S., Andrade, J., *et al.* (2011) Splicing enhances recruitment of methyltransferase HYPB/Setd2 and methylation of histone H3 Lys36. *Nat. Struct. Mol. Biol.* **18**, 977–983
103. Westendorf, J. M., Konstantinov, K. N., Wormsley, S., Shu, M.-D., Matsumoto-Taniura, N., Pirollet, F., *et al.* (1998) M phase phosphoprotein 10 is a human U3 small nucleolar ribonucleoprotein component. *Mol. Biol. Cell* **9**, 437–449
104. Morello, L. G., Coltri, P. P., Quaresma, A. J. C., Simabuco, F. M., Silva, T. C. L., Singh, G., *et al.* (2011) The human nucleolar protein FTSJ3 associates with NIP7 and functions in pre-rRNA processing. *PLoS One* **6**, 1–14
105. Strezoska, Ž., Pestov, D. G., and Lau, L. F. (2000) Bop1 is a mouse WD40 repeat nucleolar protein involved in 28S and 5.8S rRNA processing and 60S ribosome biogenesis. *Mol. Cell. Biol.* **20**, 5516–5528